CHAPTER 1

Introduction

1.1 Background

As the popularization of flat panel displays grows up, liquid-crystal displays (LCDs) have become the most common system in many commercial applications. In Fig. 1-1 shows TFT-LCDs have exceeded CRT in revenue since 2002, and the revenue of TFT-LCDs is increasing significantly year by year. It is not difficult to see that the TFT-LCD technology has emerged as the dominant display [1].

In past few years, the focus of display technology development has shifted gradually away from the TFT-array process to the so-called high-value added display. The smart panels are promoted unceasingly, for example, the touch panels used commonly in PDAs or ATM, and with the idea of energy conservation, the displays with power saving function are very popular recently [2].

As mention above, low power consumption is very important. Portable consumer electronic products, such as mobile phone, PDA etc., always move toward a tendency of constantly reducing their power consumption because users expect that they can operate for a long time. For LCD-based products, 90% power consumption is attributed to backlight [3]; accordingly, backlight power saving is considered one of the most effective ways to reduce LCD energy dissipation. In recent years, LED backlighting was sought to replace the fluorescent backlighting because the TFT-LCDs with LED backlighting have advantages of greater efficiency, long lifetime and environmental compatibility. Many researcher have paid effort to LED backlight dimming technologies to achieve power saving and contrast enhancement

[4].

1.2 Motivation

Since the LED backlight modules could be non-uniform in large panel or degrade after a long time operation, even the using of local dimming technology [5]. These situations all have the same phenomenon that is the changing of backlight intensity. In this thesis, we proposed the backlight sensor for the accurate backlight intensity. For example, the local dimming technology means that it can adjust its backlight intensity according to the frame which would be showed. Fig. 1-2 is the schematic of backlight local dimming. Then, we can use the backlight sensors to detect the light intensity, and determine the intensity whether or not to achieve the value that it should be.

The conventional a-Si TFTs can detect front light [6-7], but can not sense the backlight because of the shielding gate metal. We review the light sensing circuit proposed by S. H. Kim et al. is also about the backlight sensor [8]. Fig. 1-3 shows the light sensor which is composed of 2T1C. T1 is the switch TFT, TP1 is the photo sensor, and the Cst is the storage capacitor. For sensing backlight, they use top gate structure TFT. The gate insulator of top gate TFT is passivation layer. For sensing the backlight intensity accurately, the thickness of passivation layer must be controlled carefully.

To avoid the usage of top gate TFT, we try to use another non-conventional structure to be the sensing device, and it has the same fabrication processes as conventional a-Si:H TFTs, Thus, the light sensor can be integrated in panel without changing the mask number and extra cost. The photo effect of device will be analyzed in chapter2, and the proposed light sensing circuit will be discussed in chapter3.

1.3 Thesis Organization

CHAPTER 1 Introduction

1.1Background

1.2 Motivation

1.3 Thesis Organization

CHAPTER 2 Photo Effect of Device

2.1 Fabrication Procedure of Amorphous Silicon TFT

2.2 Photo Characteristic of Device

2.3 Summary

CHAPTER 3 Light Sensing Circuit on TFT-LCD

3.1 Conventional Light Sensing Circuit

3.2 Light Sensing Circuit and Operation Principle

3.3 Simulation

3.3.1 Simulation Method

3.3.2 Simulation Results

3.4 Digitization

CHAPTER 4 Error Factors

4.1 Device Uniformity

4.1.1 On Current Variation

4.1.2 Threshold Voltage Shift

4.2 Temperature

4.3 Reliability

4.3.1 Staebler-Wronski Effect on Device

4.3.2 The Calibration of Staebler-Wronski Effect

4.3.3 The SW Effect with Backlight Variation

CHAPTER 5 Conclusion

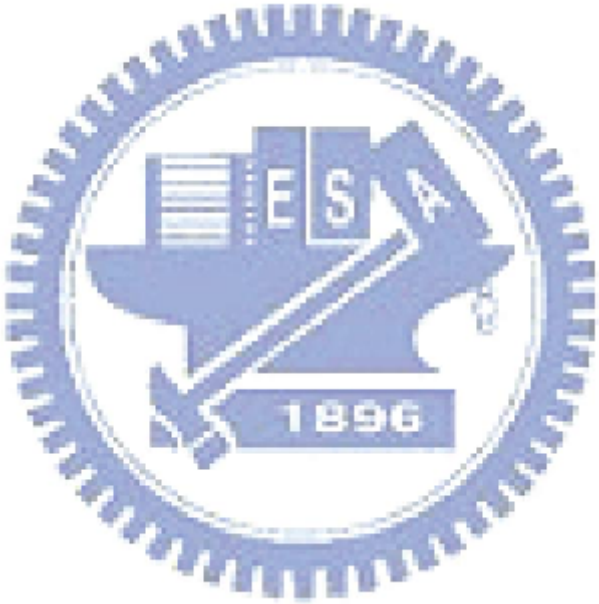

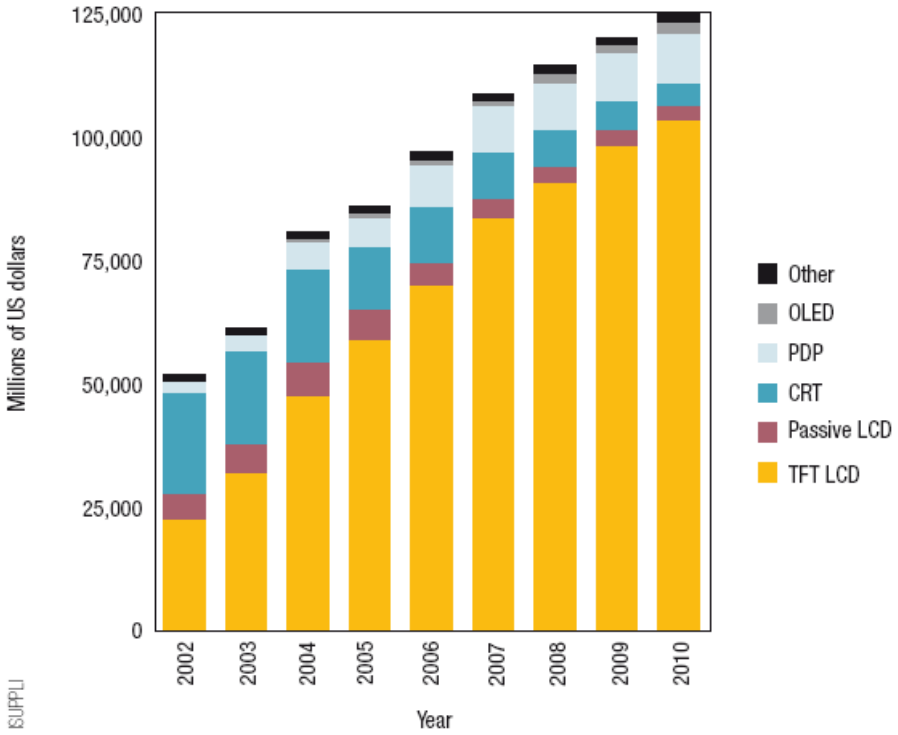

Fig. 1-1 The revenue of display from 2002 to 2010

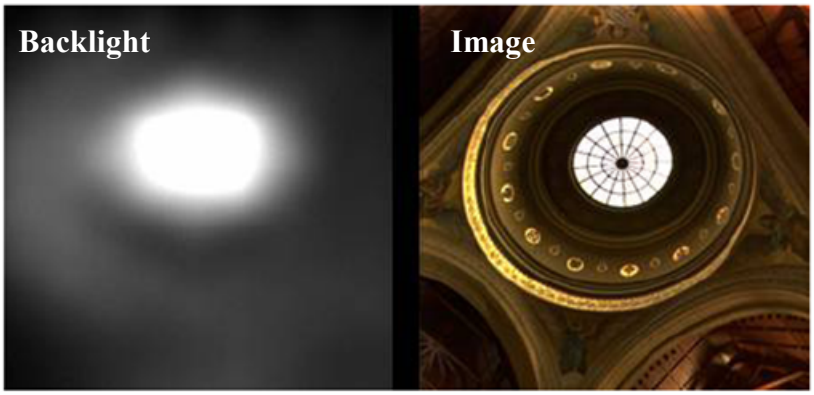

Fig. 1-2 Schematic of local dimming function by LED backlight

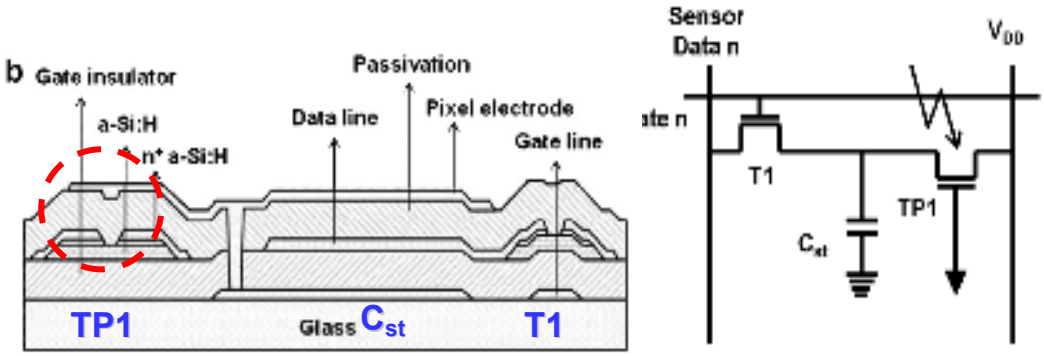

Fig.1-3 The backlight sensor proposed by S. H. Kim

[*Ref. Solid-State Electronics, 2007, pp.478-481*]

CHAPTER2

Photo Effect of Device

2.1 Fabrication Procedure of Amorphous Silicon TFT

In this study, the considered sensing device takes advantage of the same a-Si technology used to fabricate the display. Fig. 2-1 shows cross-section of conventional structure TFT and the non-conventional structure TFT. The difference is that the non-conventional structure TFT has a gap. The gap exists between bottom metal (gate) and one of top metal (source or drain), and we defined the gap size as i, so we called this structure TFT as "gap-type TFT" [9]. The basic process flow is described as follows. After the deposition and patterning of gate metal on the glass substrates, three layers, i.e., silicon nitride (SiNx, 3500 Å), a-Si:H, and n+ a-Si:H films, were successively deposited in a plasma enhanced chemical vapor deposition (PECVD) system. After making the source/drain electrodes, the n+ a-Si:H region with length (L) of 5 μm between the source/drain electrodes was etched off by a reactive ion etch. Then, a passivation layer was used to cap the channel region.

2.2 Photo Characteristic of Device

Fig.2-2 shows the transfer characteristics of conventional TFT. We find that the conventional TFT does not have any photo reaction. This phenomenon is easy to figure out from the insert diagram in Fig. 2-2. The gate metal blocked all the possible backlight which would illuminate on active layer, so it would rather said it does not be illuminated than no photo reaction. Therefore, the conventional TFT does not be

considered to be our backlight sensing device.

The transfer characteristics of gap-type TFTs (i=30um) are showed in Fig. 2-3. Since the gap-type TFT is asymmetric, it can be alternatively operated. Fig.2-3(a) is the gate-near-drain one, and Fig. 2-3(b) is the gate-near-source one. For further discussion, we define the ratio of the TFT drain current under illumination (I_{D_illum}) to that in the dark (I_{D_dark}) as $R_{L/D} = I_{D\_illum} / I_{D\_dark}$ [10]. We can find that the $R_{L/D}$ of the gate-near-source one is larger not only in OFF region (Vgs = -10V) but also in ON region (Vgs = 10V). In aspect of application, the gate-near-source one has better photosensitivity to be the sensing device. From Fig. 2-3(b), we can see its $R_{L/D}$ can achieve to 4 orders both in OFF region and ON region.

For practical application, the operating region of sensing device should be properly. Thus, we take further steps to compare the operating region for backlight sensing. Fig. 2-4 shows the OFF current and ON current versus the backlight intensity. They can not be compared directly because of the different current levels. To analyze in detail of the photosensitivity, firstly, we normalized the curves of Fig. 2-4 (a) (b). And the result is showed in Fig. 2-5(a). Next, we differentiate the normalized current to the illumination intensity. Then, the relative photosensitivity versus illumination intensity is showed in Fig. 2-5(b). There is an intersection point at about 10000 lux. It means that the sensing device operated in ON region has better photosensitivity under 10000 lux illumination. On the contrary, the device operated in OFF region has better photosensitivity above 10000 lux. On the basis of the following reasons, we decided to operate the sensing device in ON region to sensing backlight. In TFT-LCD, backlight must pass through the polarizer and then achieve the TFT array layer. The actual backlight intensity illuminate on the TFT array would not over 10000 lux. And we just know that ON region has better photosensitivity under 10000 lux illumination. Another reason for choosing ON region is the higher current level. The ON current is

higher about 2 orders than OFF current. The higher current signal can reduce the effect of noise and be read easily.

The non-conventional TFT can detect the backlight because of the gap exists. Fig. 2-6 shows the transfer characteristics of the gate-near-source TFT with different gap size (i = 5um、12um、30um). When the gap increases, the photosensitivity will be higher in ON region. Theoretically, we will use the gap as large as possible for great backlight sensing, but it will reduce the pixel aperture ratio. Base on the actual consideration, the following experiments that we all use the gap size i = 30um to be the experimental devices.

For further understanding of the relation between the gap and the photo effect, we design different structures of gate-near-source TFT. Fig. 2-7(a) shows the new structures. We can see that there are two gates in the new one. The function of the extra gate is to shield the backlight illumination. Thus, the extra gate does not be given any bias, in other words, it is floating. Next, we define "Open-ratio" to name the new structures. For example, the original structure which gap can be illuminated entirely then we call it open-100%. If the area of gap is shielded 67% from backlight illumination by floating gate, then we call it open-33%. Fig. 2-7(b) shows the relation between I_{D_illum} and open-ratio. We find that I_{D_illum} is proportional to the open-ratio. It means that the photo effect is proportional to the illuminated area of the gap.

2.3 Summary

According to the experiments mentioned above, the most obvious photo effect is observed in the gate-near-source TFT. Furthermore, its ON region is more suitable to be light sensing than OFF region. We also find that the photo effect is proportional to the illuminated area of the gap. Therefore, a proper sensing device can be selected.

However, we need to consider the unique SW effect in a-Si:H material carefully. For practical usage, a-Si TFTs are found to suffer from serious Staebler-Wronski effect (SW effect) which results from the formation of dangling bonds by breaking the weak bounds of the hydrogen atoms to the silicon, and it will decrease the lifetime of excess carriers and thus reduce the photoconductivity [11]. Therefore, it is very difficult to get a reliable sensing performance since the sensor performance changes with device photosensitivity. In chapter4, we will propose a calibration method to reduce the error from SW effect.

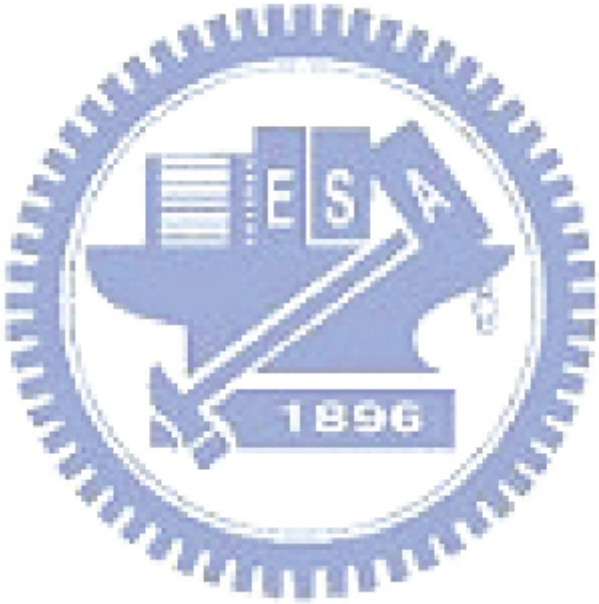

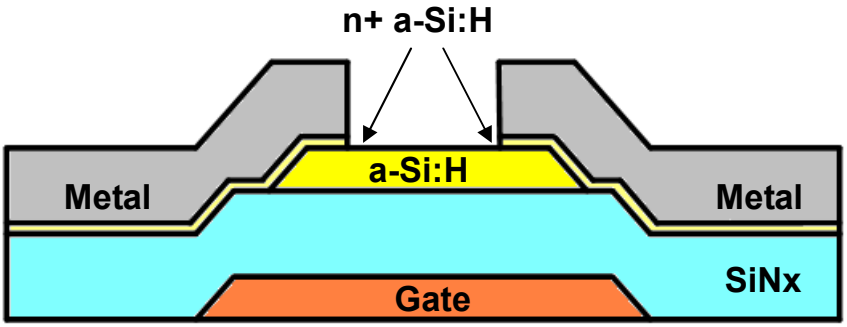

(a)

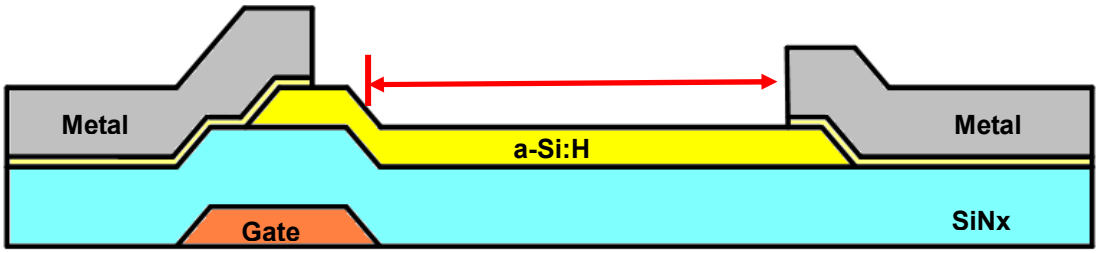

(b)

Fig.2-1 Cross-section views of a-Si:H TFT

(a) Conventional structure (b) Gap-Type Structure

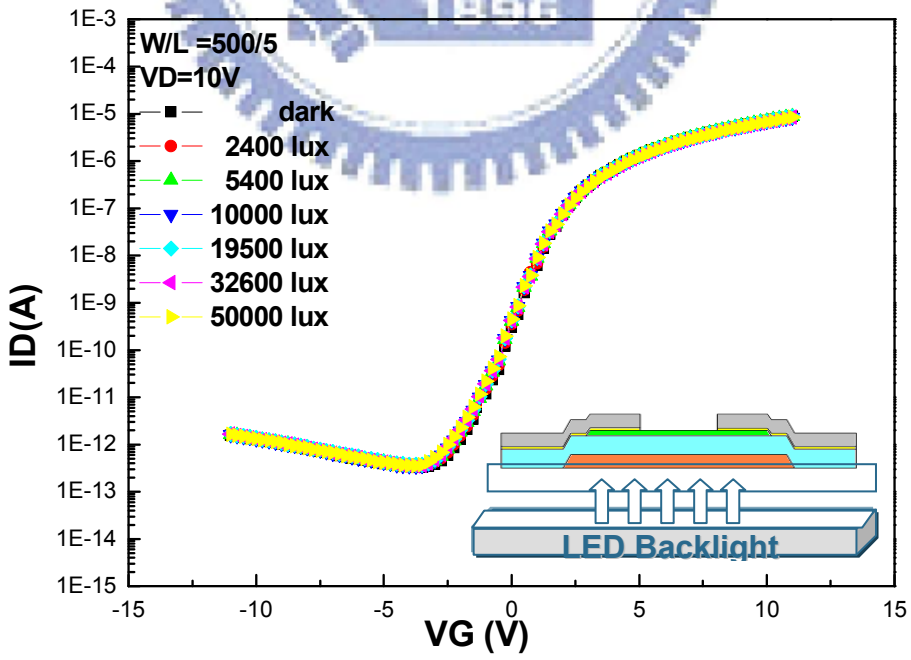

Fig.2-2 Transfer characteristics of conventional a-Si TFT

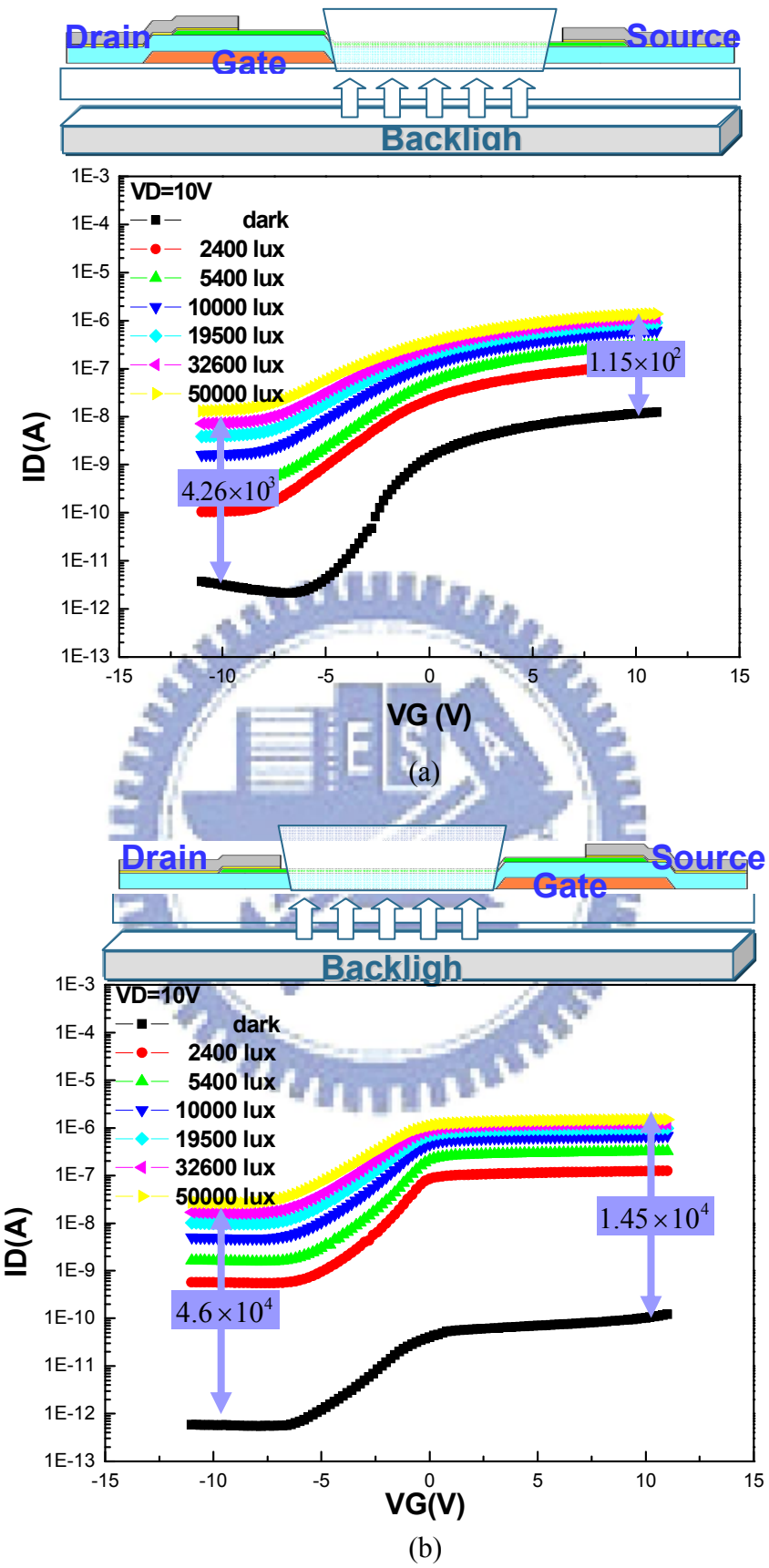

Fig.2-3 Transfer characteristics of gap-type TFT

(a) The gate-near-drain TFT (b) The gate-near-source TFT

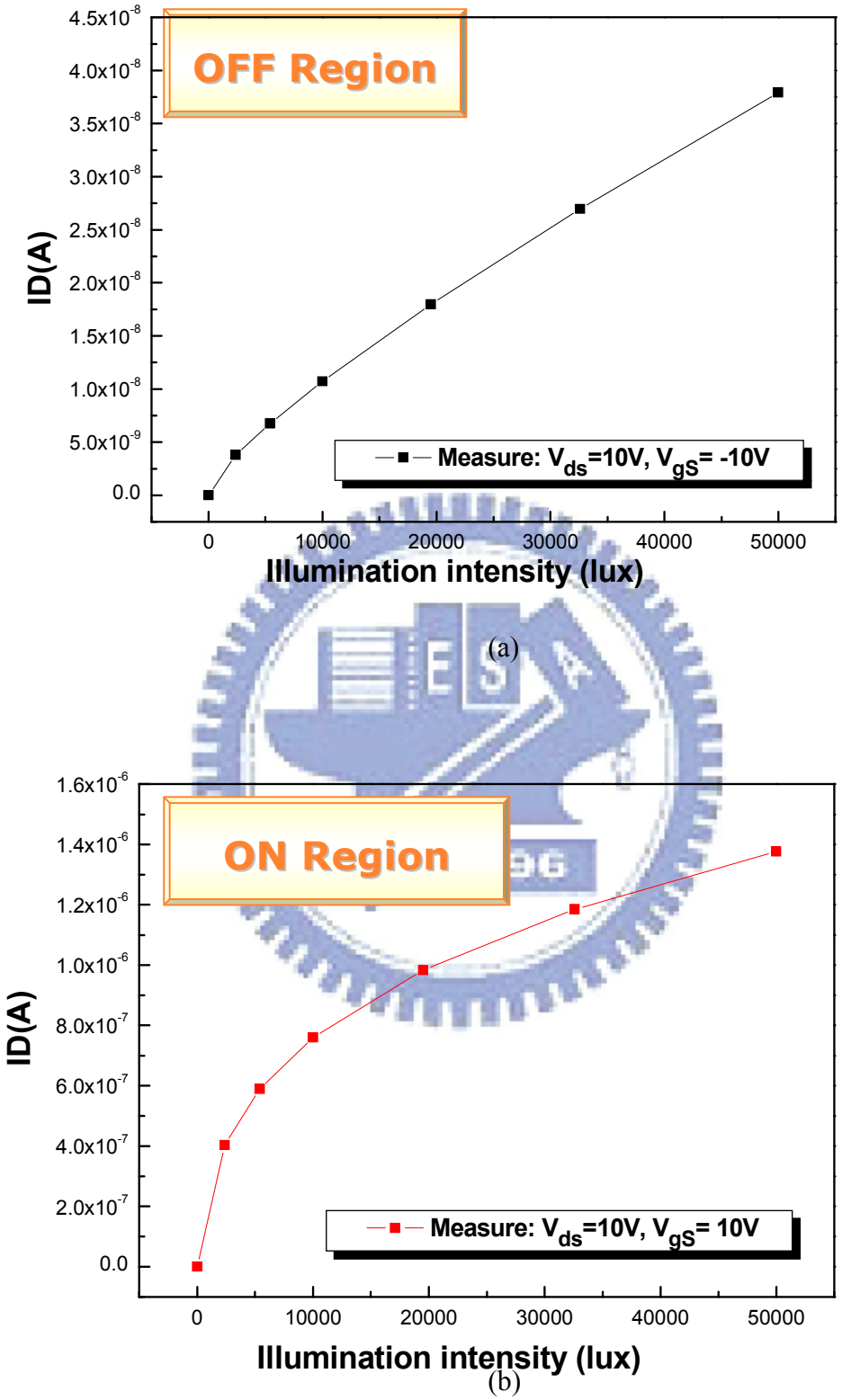

Fig.2-4 Drain current versus backlight illumination intensity

(a) in OFF region (b) in ON region

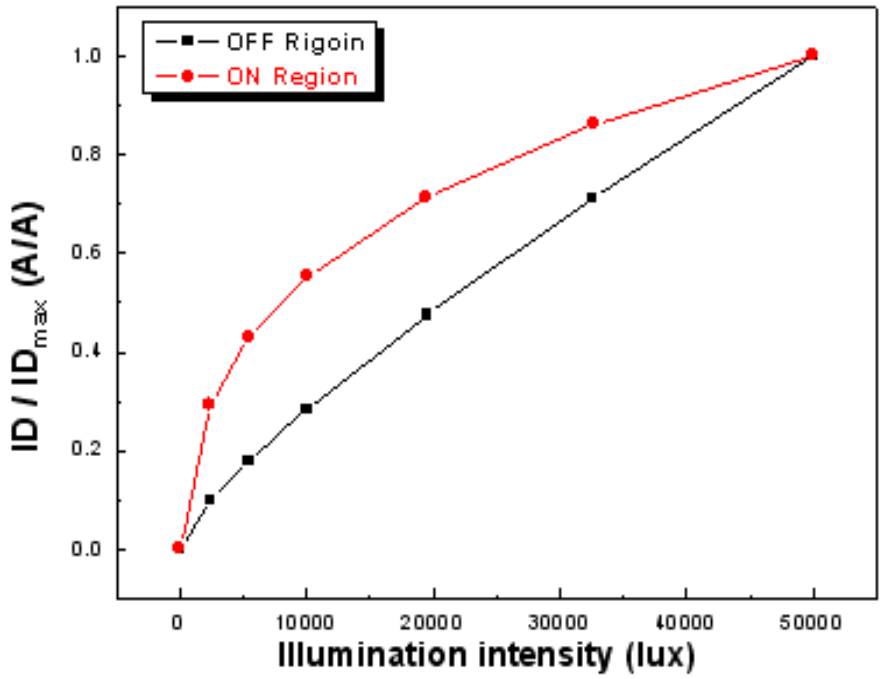

(a)

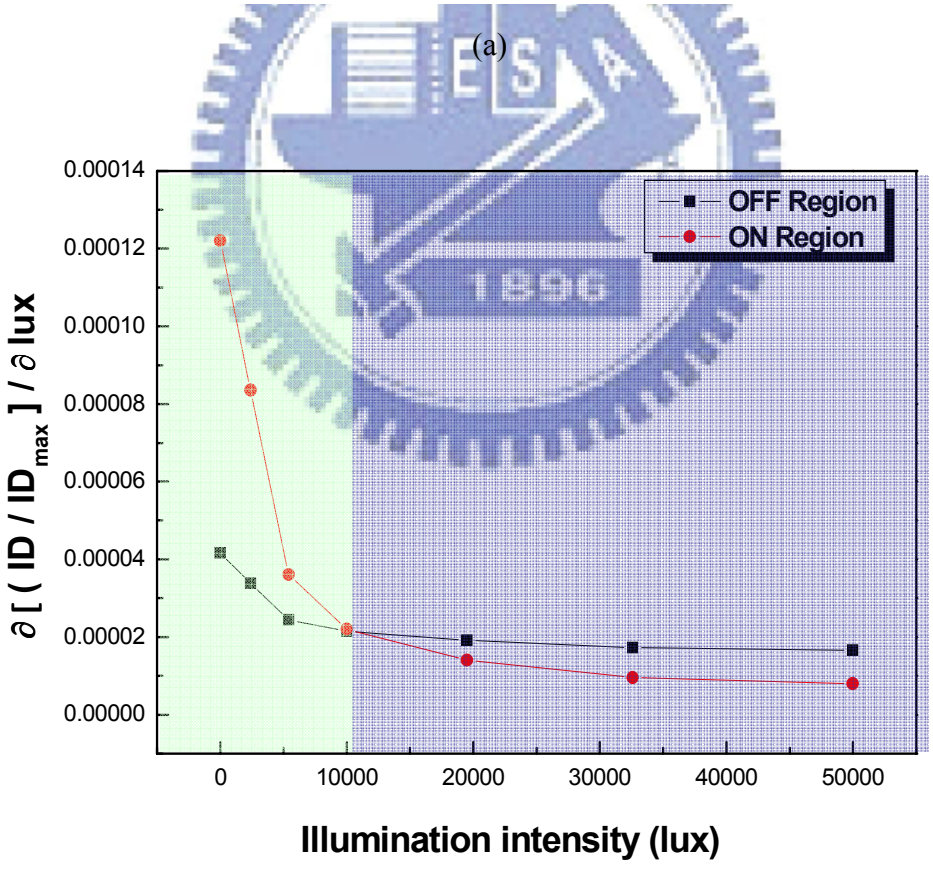

(b)

Fig.2-5(a) The normalized drain current versus backlight illumination intensity of ON region and OFF region (b) The relative photosensitivity of ON region and OFF region

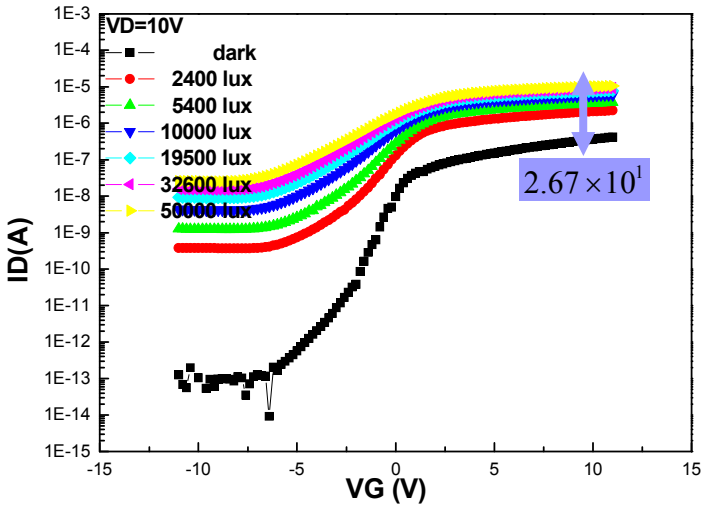

(i)

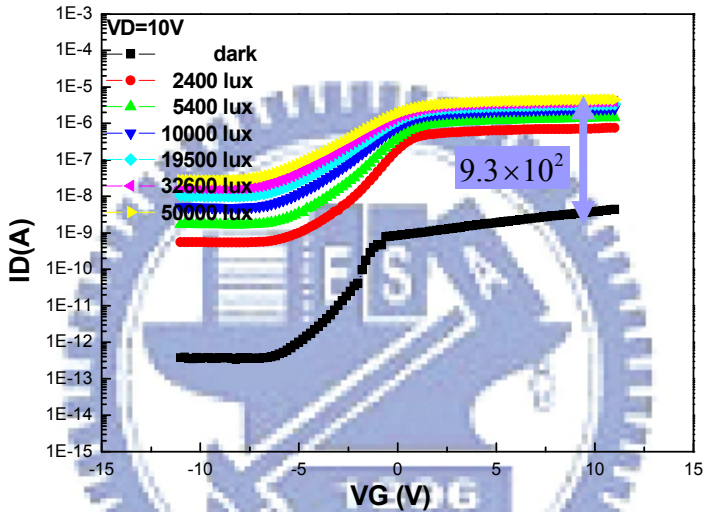

(ii)

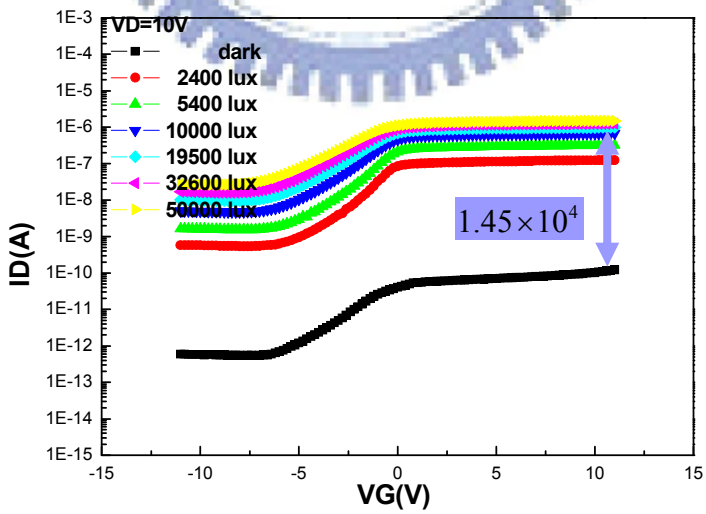

(iii)

Fig.2-6 Transfer characteristics of gap-type TFT with different gap sizes

(i) i = 5um (ii) i = 12um (iii) i = 30um

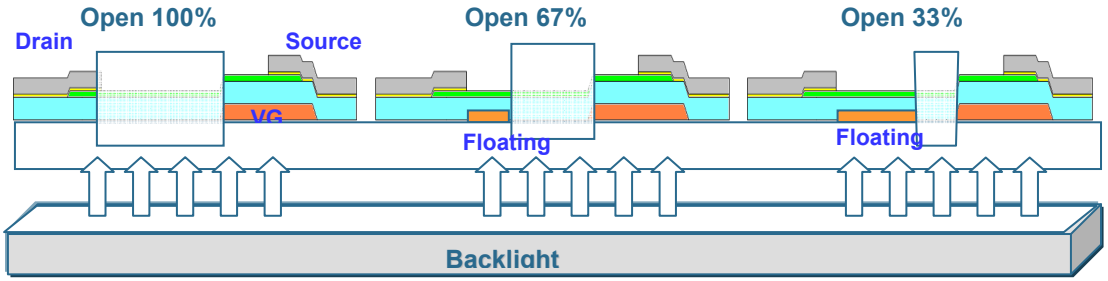

(a)

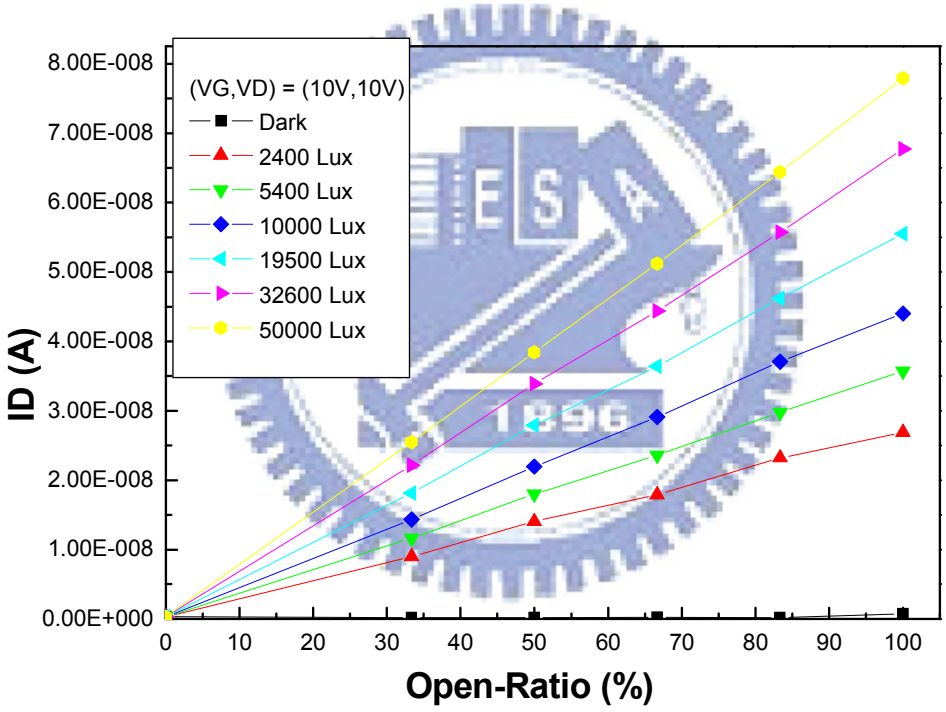

(b)

Fig.2-7 (a) Schematic diagram of different open-ratio structures

(b) Drain current versus open-ratio

CHAPTER 3

Light Sensing Circuit on TFT-LCD

After the discussion of the photo effect in chapter 2, we decide to use on region current as the signal of illuminated intensity, and focus on its photo characteristic. Therefore, we propose a backlight sensor which can sense the changes of on region current at different backlight intensities, and the sensor is compatible to panel's scan line.

3.1 Conventional Light Sensing Circuit

In conventional design, we use 1T1C to compose a sensing circuit which is showed in Fig. 3-1. The operating principles can be described as two periods shown in the timing diagram. In the charge period (1), when gate signal becomes "high", T1 TFT is turned on. Thereby, the input voltage (V_{in}) "high" is stored in C_s and the voltage of node A (V_A) is charged to "V_{in_high}". In the discharge period (2), the gate voltage of T1 is applied so that T1 is operating in the OFF region while sensing operation. At the same time, V_{in} becomes "low". The photo leakage current drained away through the T1. The V_A is discharged by the photo leakage current of T1.

We added a TFT (T2) to be a source follower readout part as shown in Fig. 3-2. A 2T1C light-sensing circuit and its timing sequence have been proposed. The readout part is used to convert the photo leakage current to analog voltage signal, which is more easily processed by the peripheral circuit. Among several ways to achieve this purpose, the first method coming to mind is using an operational amplifier (OP-Amp). However, the OP-Amp is hard to be implemented by a-Si TFT technology and integrated into pixel. Therefore, we use only one TFT as source follower to do that [12, 13].

The proposed 2T1C sensor has been fabricated on the glass substrate using a-Si technology for verification of light-sensing operation as shown in figure 3-3. Since the photo transistor of conventional circuit is designed as conventional TFT, we only can sense front light to verify light-sensing operation. The output voltage of the proposed circuit is measured by oscilloscope during discharge period under illumination and in the dark. The output waveforms are shown in figure 3-4(a) and (b). The discharging rate of V_{out} which is due to photo leakage current can be expressed as dV/dt. In 1390 lux illumination, the dV/dt is 40 (=2V/0.05sec) with Cs equals to 6pF. This discharging rate corresponds to the current value is $2.4x10^{-10}$A. It is close to the current value 1.98 $x10^{-10}$A, which is measured from device under 1390 lux. That means the different light intensities can cause different photo currents, and the different photo current levels will response to the different discharging rates. This fact proves that we can indeed detect light intensity by such a sensing circuit composes of a sensing TFT and a storage capacitor.

3.2 Light Sensing Circuit and Operation Principle

Following, we propose a new light sensing circuit which is designed to integrate into pixel. As described in chapter 2, this circuit will operate the sensing device, gate-type TFT, in ON region.

3.2.1 Circuit Structure and Operation Principle

Fig.3-5(a) shows the proposed 4T2C circuit, and it includes a sensing part and a readout part. The sensing part is composed of a reset TFT, a photo TFT, and two capacitors, Cc and Cs. The readout part is composed of a source follower and a switch TFT.

The operating principles can be described as two periods shown in Fig. 3-5(b). In

the reset period (1), scan line1 signal becomes “high”, the reset TFT is turned on. Thereby, the voltage of node A is charged to V_{com}. In the discharging period (2), the scan line1 signal becomes “low”, reset TFT is turned off. Meanwhile, the scan line 2 signal becomes “high”, the photo TFT is operated in ON region. At the same time, the voltage of node A rise to a relatively high voltage to V_{com} owing to the couple effect from the voltage changing of scan line 2 through Cs. Then, the photo current, which is determined by the intensity of the illumination, drained away through the photo TFT. The V_A would be discharged by the photo current of photo TFT, and then voltage change at node A can be followed by source follower, and readout through switch TFT line by line. The Cc is especially added to divide voltage of node A to a proper V_D for photo TFT when coupling happened. Meanwhile, it can make sure the voltage at node A be lower than the drain voltage of source follower (Vg,on in our case) for its properly working.

3.3 Simulation

The proposed 4T2C light-sensing circuit is simulated.

3.3.1 Simulated Method

In the RPI models of TFT, there is no photo current model for SPICE simulation [14], so we can not simulate the photo current under different illumination directly. We have to modify the simulation method according to illuminated characteristics of device. Figure 3-6 shows the illumination dependence of I_D-V_D characteristics curve; the drain current increased while the illumination intensity enhanced. Then, we fit the curve in the formula, which can be expressed as “$I_D = I_0(L) + A_0(L) \times V_D$”. Where $I_0(L)$ and $A_0(L)$ are intercept and slope, which are illumination dependent. Therefore, we use the different current sources and resistors in parallel to represent the different

photo currents of TFT. Table 3-1 shows the values of $I_0(L)$ and $R_0 = 1/ A_0(L)$ at V_{gs}=10V at different illumination intensities. For the simulation at different illumination intensities, we change the value of $I_0(L)$ and R_0 accordingly.

3.3.2 Simulated Results

Firstly, we focus on the readout part. The simulation result in Fig. 3-7 shows that Vout is just lower than Vin by the threshold voltage (Vt) of the source follower, and it functions well at panel's scan period (~16us).

Fig. 3-8 shows the SPICE simulation results of light sensing circuit, and Table 3-2 lists the simulation condition. The illumination intensity can be monitored by the slope of the discharging voltage.

The equivalent circuit and layout of sensor integrated in pixel are shown in Fig. 3-9. We can see the proposed light sensing circuit is compatible to panel's scan lines, and it only needs a readout line to output the signal. Taking 52" full HD panel as example, namely, pixel size of 200x600um^2 , the aperture ratio reduces from 84% (without sensor) to 78% (with sensor). The scarification in aperture is acceptable.

Another question comes to us is how dense the backlight sensors are needed to be embedded in the pixel array? Fig. 3-10 shows an example schematic of panel with local dimming function. But the actual situation must be decided according to the arrangement of the backlight modules.

3.4 Digitization

In order to restrain the interference of noise and avoid the error due to V_{th} shift of source follower, a high accuracy ADC has been proposed. The digitization circuit is shown in figure 3-11(a), which consists of two comparators, a "AND" logic gate and a counter. Two reference voltages V_{ref_1} and V_{ref_2} are used to compare with V_{out}, we

can adjust the range of V_{out} with different signals "V_{ref_1}" and "V_{ref_2}". If $V_{out} > V_{ref\_1} > V_{ref\_2}$ or $V_{ref\_1} > V_{ref\_2} > V_{out}$, the output of logic gate C is always "0", as shown in figure 3-11(b). Only when $V_{ref\_1} > V_{out} > V_{ref\_2}$, the output of logic gate C will be the clock numbers of CLK. Therefore, we can discriminate the slopes of V_{out} between different illumination intensities by counting the clock numbers. Moreover, in order to improve the resolution of the ADC, we can increase the speed of the CLK.

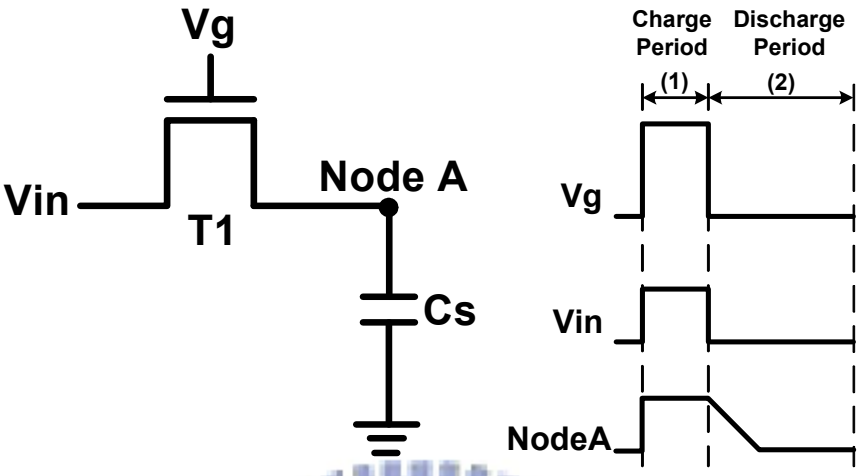

Fig.3-1 Original backlight sensing circuit design

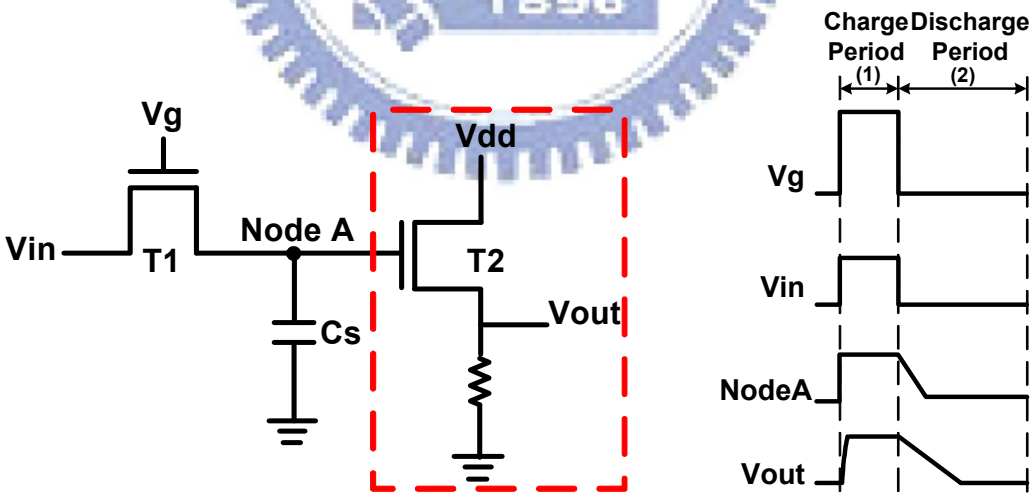

Fig.3-2 Source follower as the readout part of sensor

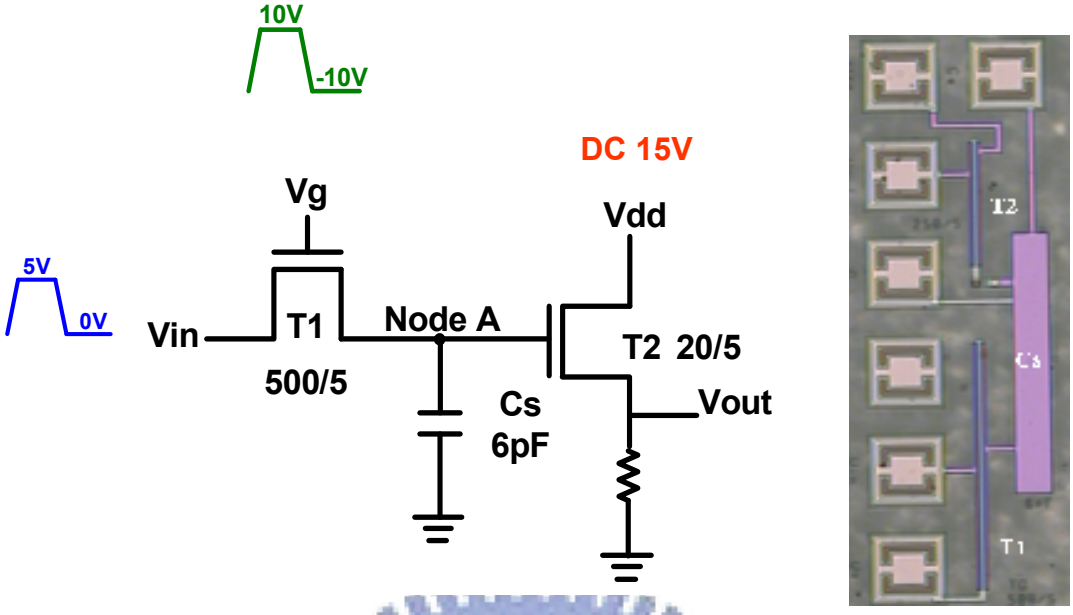

Fig.3-3 Photograph of the fabricated 2T1C light-sensing circuit

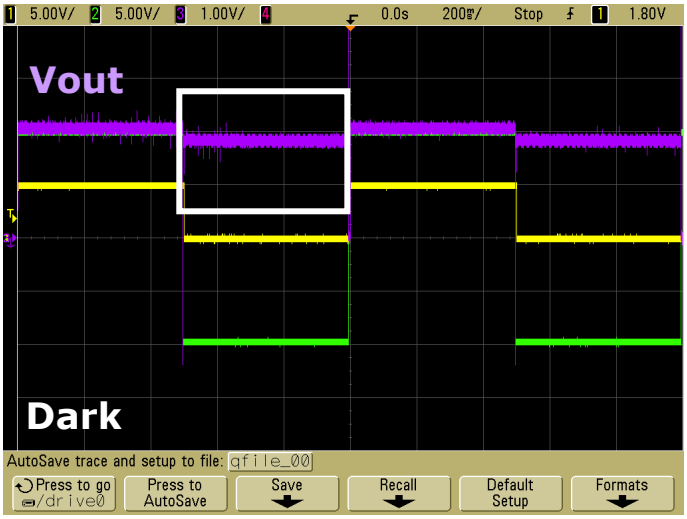

(a)

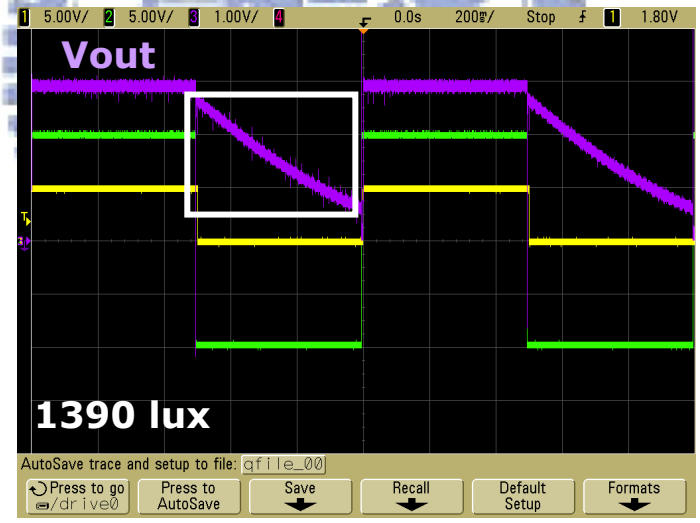

(b)

Fig.3-4 Experiment result of light sensing circuit

(a) in the dark (b) under illumination

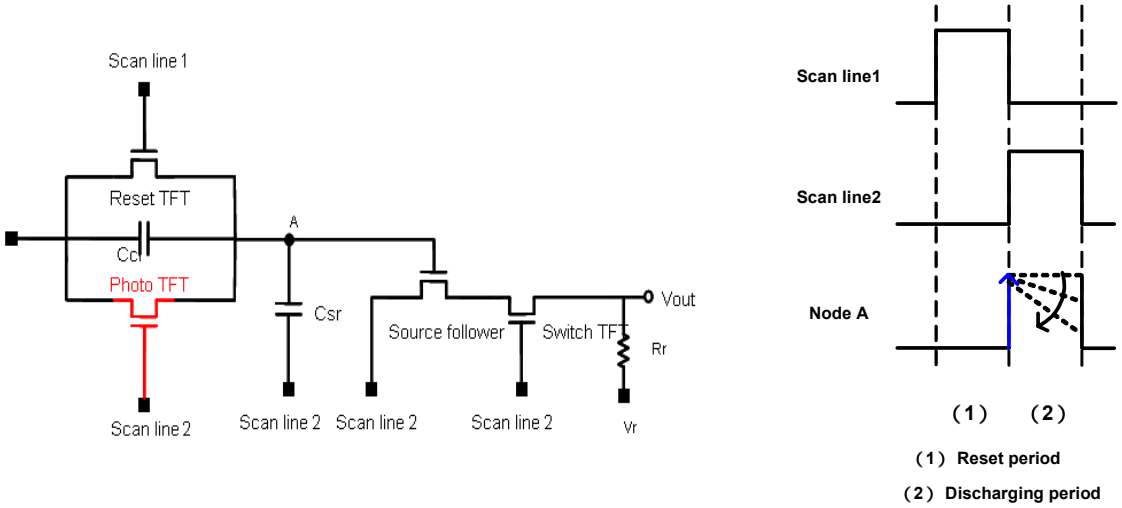

(a) (b)

Fig.3-5 (a) Proposed 4T2C light sensing circuit and (b) The time diagram

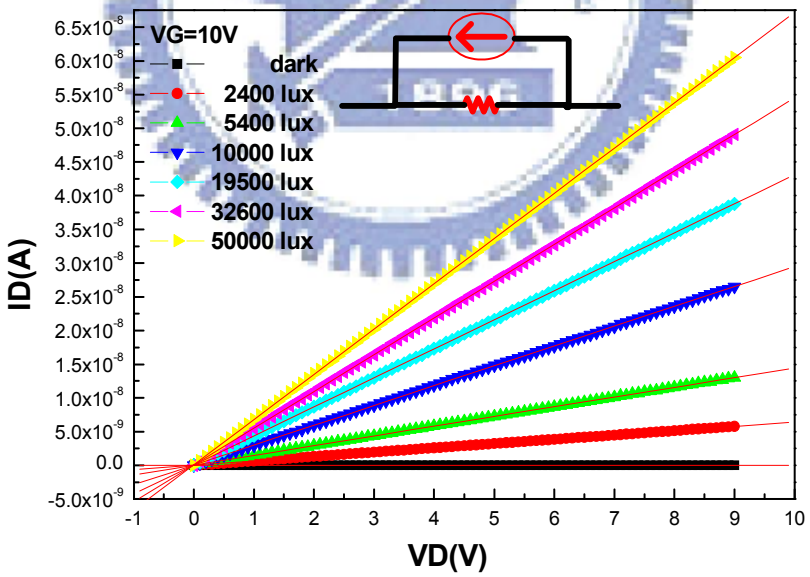

Fig.3-6 I_D-V_D curve for photo current simulation

Brightness	$I_0(L)$ [A]	R=1/A(L) [Ω]
Dark	-2.85E-13	1.61E+12
2400lx	2.22E-11	1.44E+09
5400lx	3.15E-11	6.47E+08
10000lx	6.30E-11	3.21E+08
19500lx	8.01E-11	2.21E+08
32600lx	7.95E-11	1.75E+08
50000lx	7.44E-11	1.43E+08

W/L=15/5

Table3-1 $I_0(L)$ and $R_0 = 1/ A_0(L)$ at V_{GS}=10V

with the illumination intensity variation

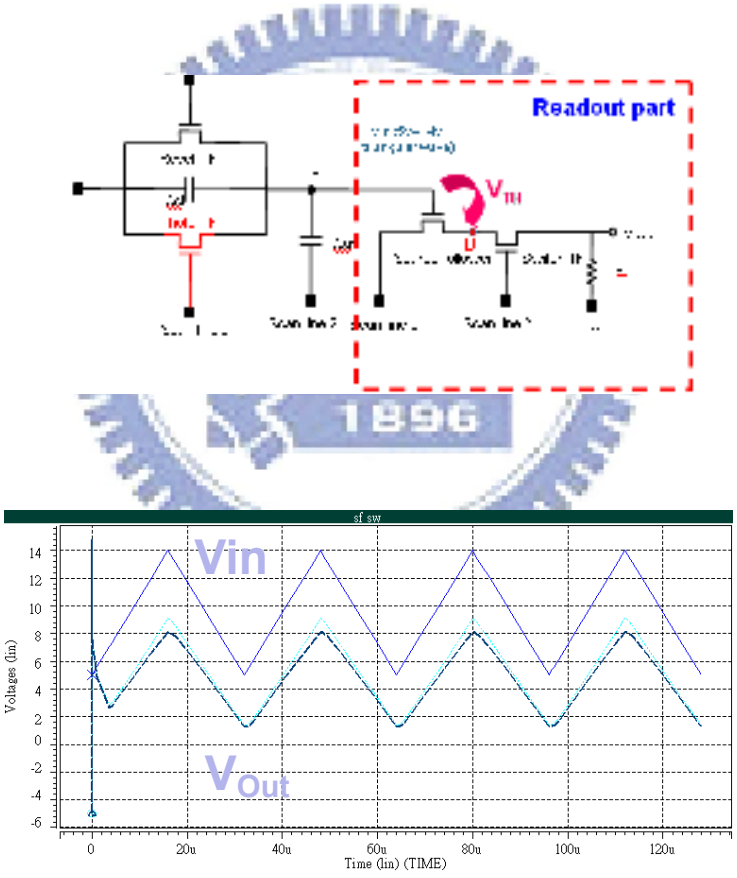

Fig.3-7 Simulation of the readout part

Feature	Specification
Operation region	ON. (V_{GS} = 10V)
Operation Period	16us
Illumination intensity	0~50000 lx
Scan line	-5V~15V
V_{com}	5V
C_{Sr}	0.012pF
C_c	0.016pF

Table 3-2 Circuit simulated conditions

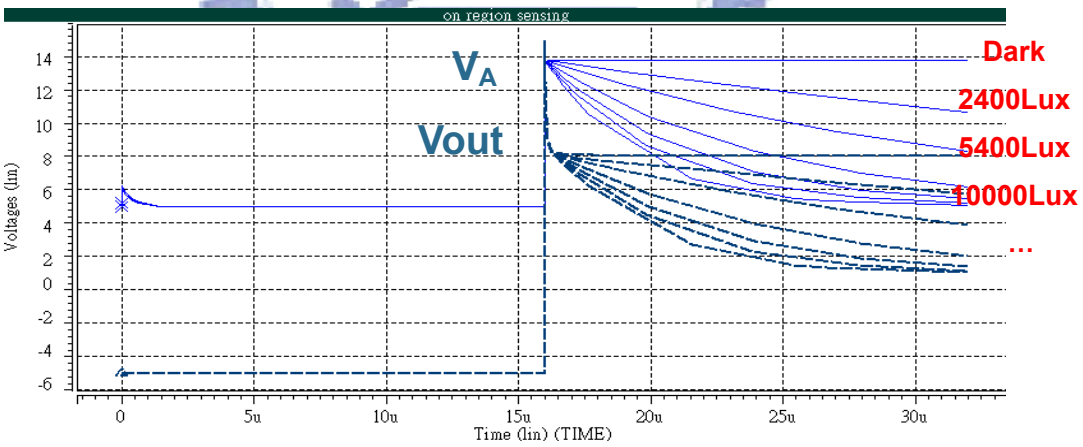

Fig.3-8 Simulation results of light sensing circuit

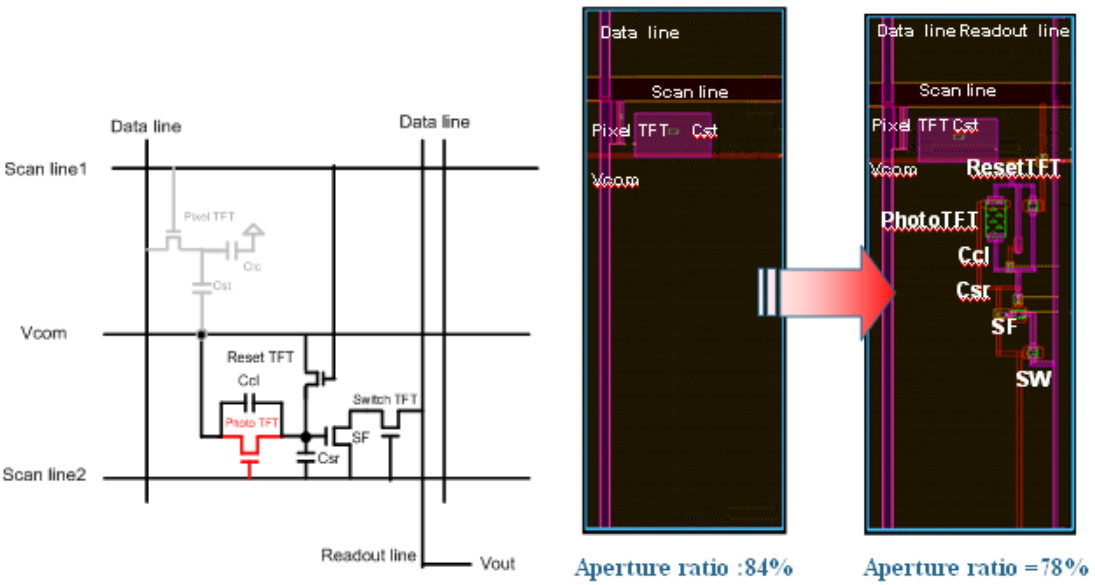

Fig.3-9 Equivalent circuit and layout of the proposed sensor

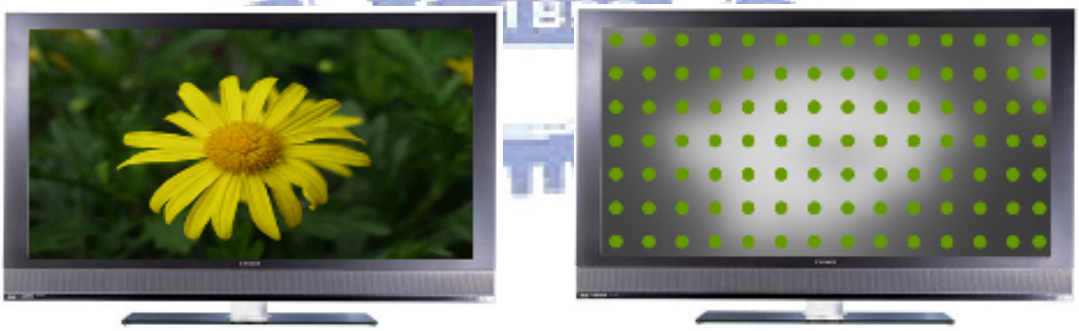

Fig.3-10 Schematic diagram of sensor array embedded in panel

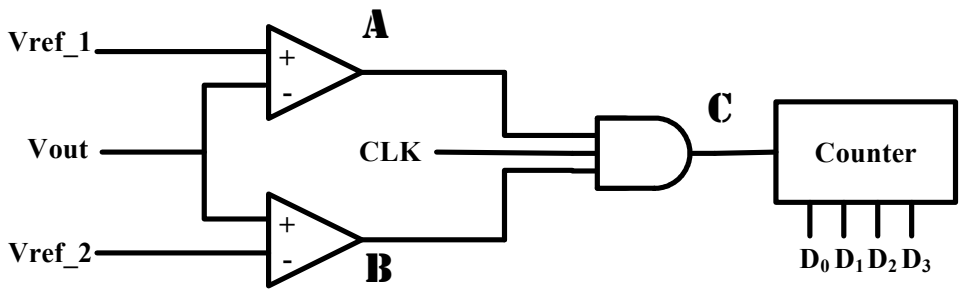

(a)

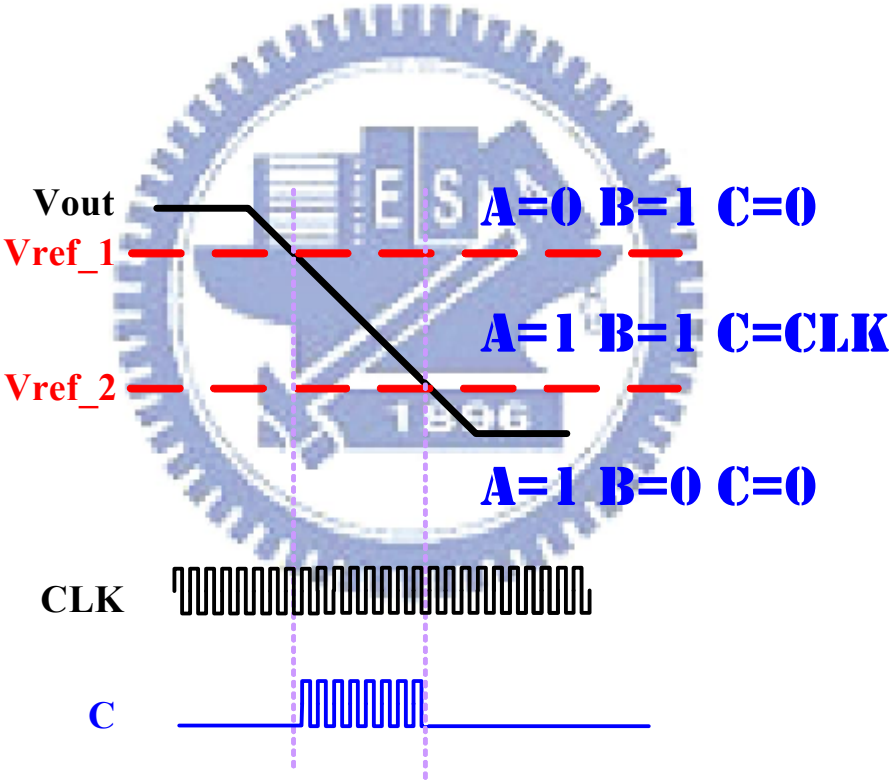

(b)

Fig. 3-11 (a) Simplified block diagram of digitization circuit and (b) its signal diagrams

CHAPTER 4

Error Factors

In this chapter we will discuss the sensing error from several possible factors, namely, device uniformity, temperature, and instability of a-Si.

4.1 Device Uniformity

In this section we consider two kinds of device uniformity issue, on current variation and Vth shift [15].

4.1.1 ON Current Variation

The measured ON currents of eight devices with respect to the illumination intensity are shown in Fig. 4-1(a). Four of them are on sample-A glass substrate and the other four are from another glass substrate sample-B. We can see the curves have some variation. And we take further steps to analyze the sensing error. Firstly, we average the eight measured currents, and take it as the reference. Next, we use the originally measured current to look up the illumination intensity according to the reference. This corresponding backlight intensity is called $Lux_{measured}$. Since it is different from the light intensity (Lux_{Real}), the device really shined, the error can be defined as "$\frac{Lux_{measured} - Lux_{Real}}{Lux_{Real}}$". Fig. 4-1(b) shows the error from the on current variation of the eight devices. It has a maximum error 7.5% at 5400 lux illumination.

4.1.2 Threshold Voltage Shift

As for V_{th} shift, we simulate its effect by changing V_{gs} low level. Fig. 4-2(a) shows the I_D at V_{gs}=9V, 10V, and 11V, which represents the influence of V_{th} shift ±1V in the case of V_{gs}=10V. We find that there has little change owing to V_{th} shift. It can

be understand from the insert diagram in Fig. 4-2(a). The diagram shows the I_{D_illum} is almost independent of the gate voltage in ON region. Similarly, we take the V_{gs}=10V as a reference, and then calculate error of the cases of the V_{gs}=9V and V_{gs}=11V corresponding to the backlight intensity. The maximum error is only 3.28%, showing that the threshold voltage shift will not cause too much influence to light sensing.

4.2 Temperature

In application, the sensor is embedded in TFT array. And the panel's internal temperature will change during usage. Thus, we need to consider the temperature effect of device. Assume 40℃ is the panel's normal operating temperature, and it is subject to ±5℃ variation. Fig. 4-3(a) shows the measured current of device-1 at 35℃、40℃ and 45℃. Calculating the error of four devices, we find the maximum error can be up to 16.4%, which can not be neglected and needs to be reduced.

Fig. 4-4(a) shows the curves of the photo drain current versus temperature. With the temperature increasing, the drain current also raises gradually [16]. We fit these curves linearly, and define the slopes as a temperature coefficient (TC). Under different illumination intensities, we can get the different TCs. It means that the device does not have the identical response to temperature under different illumination intensities. Fig. 4-4(b) further shows the relation between TC and illumination intensity for four devices. We find there is an obvious variation of temperature response from device to device. This phenomenon will make it more difficult to develop a calibration method. Therefore, for reducing the error caused by temperature variation, we propose to control the temperature of the panel instead of calibrating it. When the temperature variation is controlled within ±3.5℃, and the error can be reduced to 10%.

4.3 Device Reliability

From the study of thin-film hydrogenated amorphous silicon, it is well known that the photo current response of a-Si:H deteriorates under illumination. This property is known as the Staebler-Wronski (SW) effect. The predominant explanation of the effect is that the illumination leads to the creation of additional meta-stable states in the band gap of the amorphous silicon, by breaking the weak bounds of the hydrogen atoms to the silicon, which decreases the lifetime of excess carriers and thus reduces the photoconductivity [17,18,19].

4.3.1 Staebler-Wronski Effect on Device

To study the SW effect, we use 19160 lux backlight to illuminate the device, and the stress time is from 0 sec to 4800 sec. Fig. 4-5(a) shows the result of optical stress. We can see that with stress time increasing the current degrades obviously. And the error created by SW effect is shown in Fig 4-5(b). Compare to the other error factors, SW effect is very serious. If it is not calibrated, the device can not be applied at all. In this thesis, we will propose a method to solve this issue. Before explaining the calibration method, we want to review some content of chapter 2. In chapter 2, we mentioned the illuminated area of gap is proportional to the I_{D_illum} which is shown again in Fig. 4-6(a). After optical stress, the device with larger open-ratio will suffer from longer stress because the gap area is larger. The different stress levels will result in the nonlinear dependence of photo current on the operation as shown in Fig. 4-6(b).

4.3.2 The Calibration of Staebler-Wronski Effect

Before introducing the calibration method, we define the I_D/Open-ratio as the new index. The I_D/Open-ratio versus open-ratio before stress is shown in Fig. 4-7 (a).

We can see the I_D/Open-ratio is independent of open-ratio before stress. Since the device degraded level associates with illuminated intensity, stress time as well as illuminated area, it implies that the larger open-ratio structure will degrade more serious. Fig. 4-7(b) shows curves of the stressed devices. The one with open ratio of 100% degrades most seriously. The smaller open-ratio structure subjects to smaller influence from SW effect. The first idea coming to mind is finding open-0% structure which means it will not be stressed by backlight.

Since there is no open-0% structure of gap-type TFT, which will become conventional TFT and insensitive to backlight, we need to extrapolate it by the other structures with different open ratios. Now we explain the procedure of calibration for the sensing of the 50000 lux backlight as an example. Fig. 4-8(a) shows the curve of I_D/Open-ratio versus open ratio for various stress times. We use a formula in the form of **y=a+[b*exp^(-x/c)-1]** by OriginPro software to extrapolate the case of 0% stress. To obtain the case of 0% stress, the x, which represents open ratio, is replaced by 0. Therefore, the I_D/Open-ratio without optical stress, which is represented by y, would be the coefficient a. For various stress times, all the extrapolations give almost the same I_D/Open-ratio value of 7.73×10^{-8} ($\pm$ 1.68×10^{-9}) (A/%). Since this value is independent of stress time, we take advantage of this unique phenomenon for calibration. Looking back to refer to Fig. 4-7(a), this stress time independent I_D/Open-ratio value corresponds to the illumination intensity of 48836 ($\pm$ 2986) lux, which is very close to the real illumination intensity. For other cases, we can also use this extrapolation method to obtain the corresponding 0% cases. Then, we transfer the obtained value to corresponding light intensity according to the curve in Fig. 4-7(a). Next, we do the error analysis between the measured light intensity, also called calibrated light intensity, and the really illuminated intensity. The error defined

as $\frac{\text{Lux}_{\text{measured}} - \text{Lux}_{\text{Real}}}{\text{Lux}_{\text{Real}}}$. We can see the maximum error, shows in Fig. 4-9 (b), can be reduced from 99.2% without calibration to about 13.6%. This result indicates that the calibration method is very effective to lower the SW influence.

The values of certain parameters (a, b, c, R square) [20] are shown in Table 4-1. The values of R square are above 0.99943, which is evident that the models presented are able to fit the data accurately.

4.3.3 The SW Effect with Backlight Variation

In reality, the backlight intensity is not always fixed. Therefore, we want to verify the calibration mentioned above under changed backlight stress. From 0 to 3600 sec, the devices are stressed by l0000 lux backlight. The following 3600 sec, the devices continue to be stressed by l9160 lux backlight. Because the different stressed intensities, the curves present two different degrading speed as shown in Fig. 4-10(a). We also use the same proposed method to calibrate SW effect. The error analysis shows in Fig. 4-10(b) tell us that the proposed calibration method still can calibrate the SW effect effectively under actual backlight illuminating situation.

4.4 Summary

We discuss the sensing error from several possible factors in this chapter, including the device uniformity, temperature, and SW effect. Fig. 4-11 shows the maximum error from each factor. It can be seen that the SW effect is the most serious problem and can be reduced obviously by the calibration method.

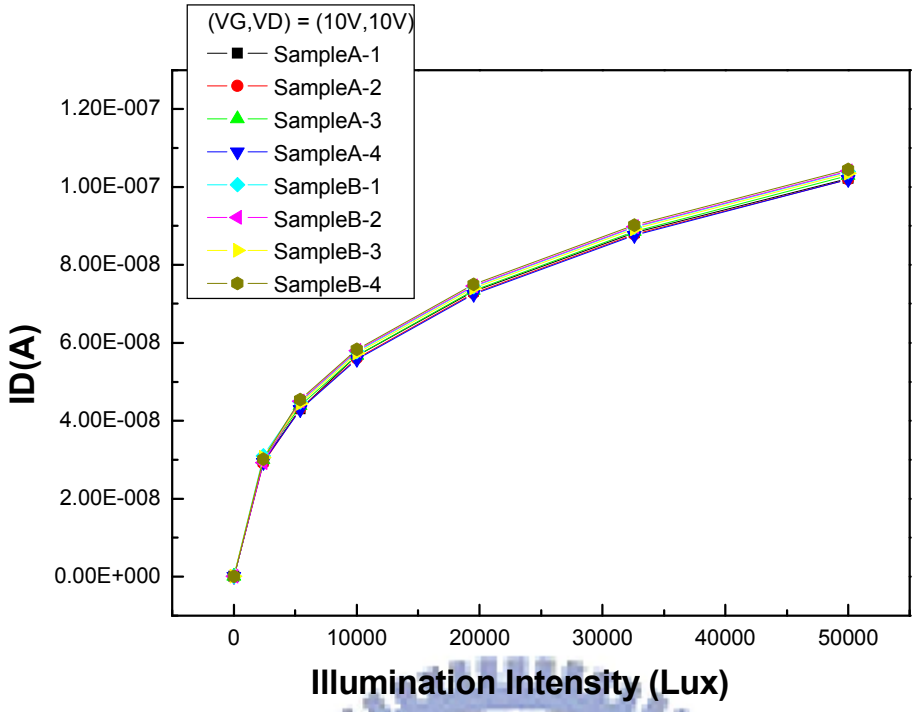

(a)

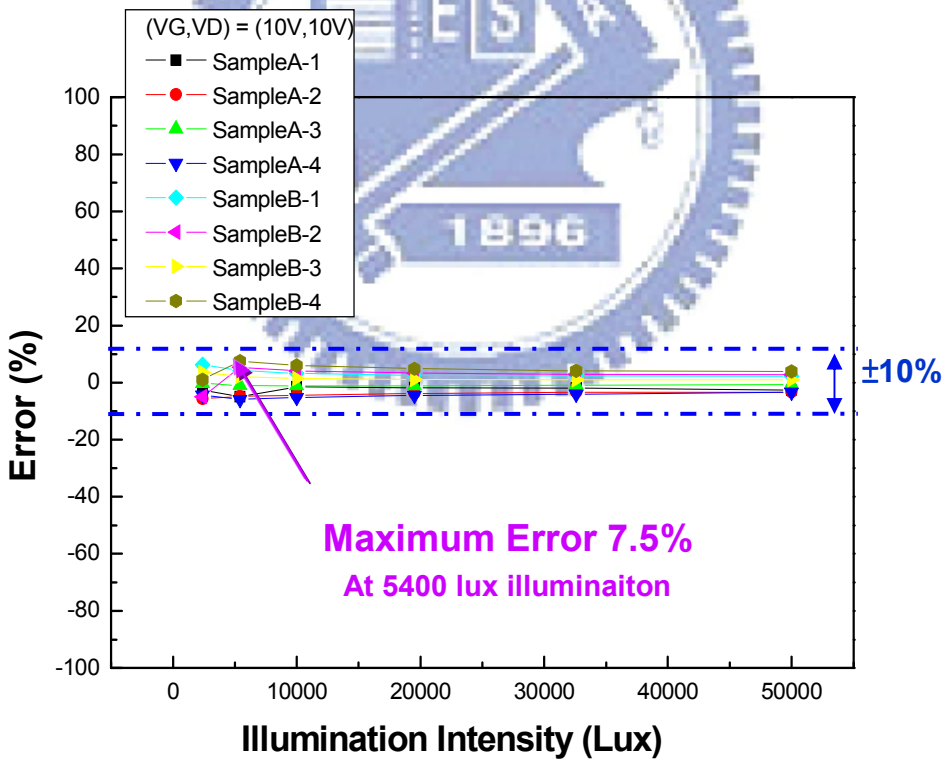

(b)

Fig. 4-1 (a) The drain current versus illumination intensity curves of 8 devices and (b) Error analysis of on current variation between the measured light intensity and the illuminated light intensity

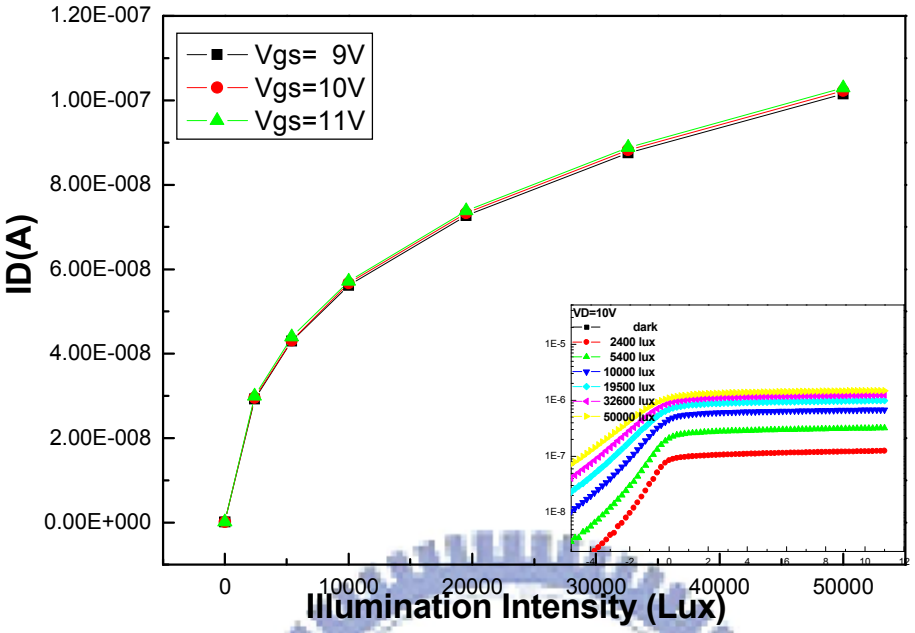

(a)

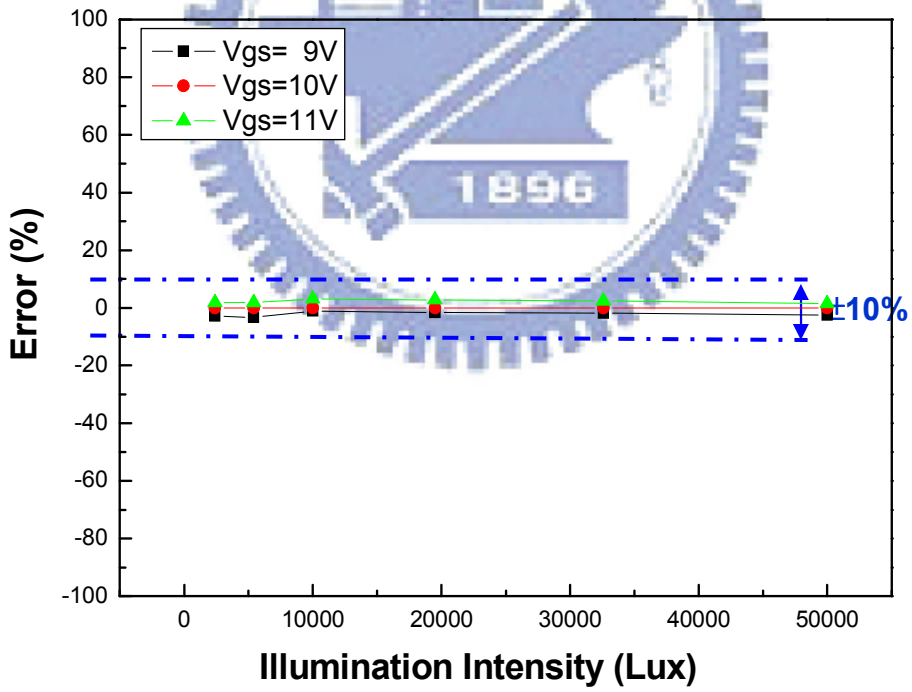

(b)

Fig. 4-2 (a) The drain current versus illumination intensity at Vgs = 9,10,11V and (b) Error analysis of threshold voltage shift between the measured light

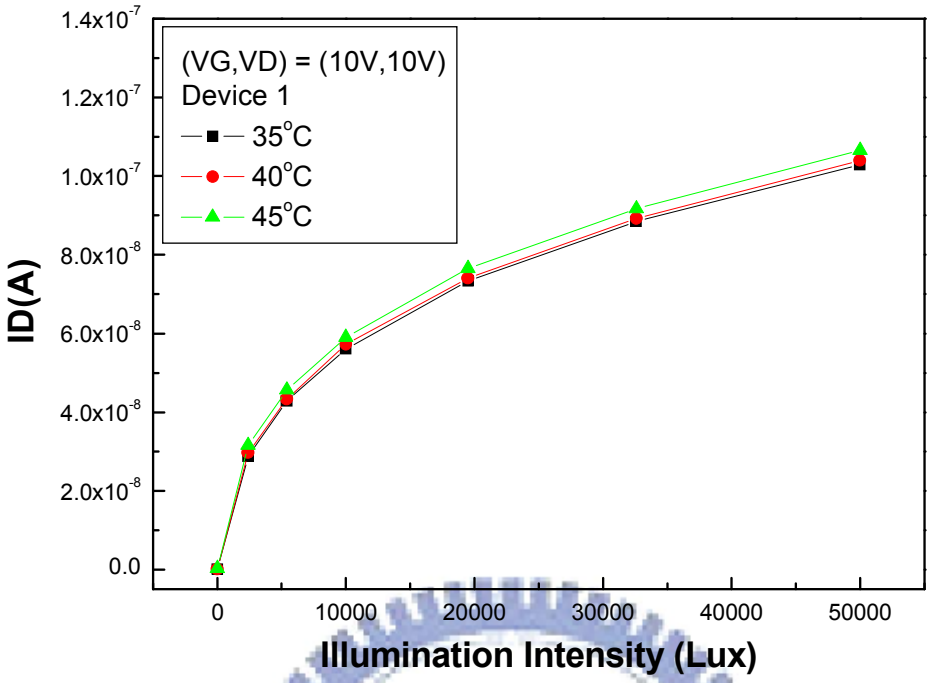

(a)

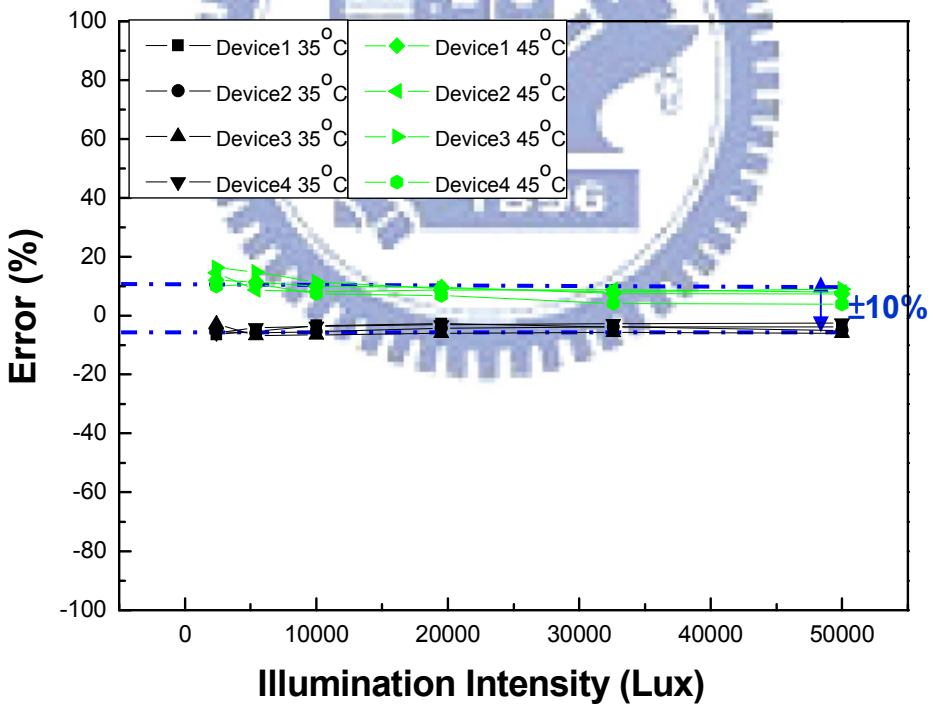

(b)

Fig. 4-3 (a) The drain current versus illumination intensity at T = 35,40, 45 ℃ and (b) Error analysis of temperature variation between the measured light intensity and the illuminated light intensity

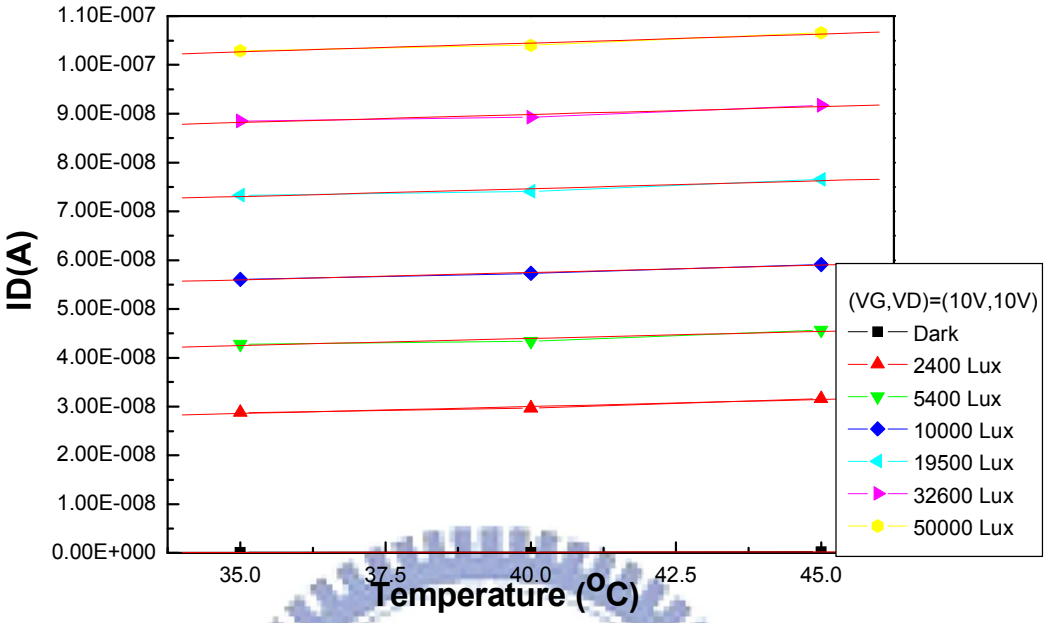

(a)

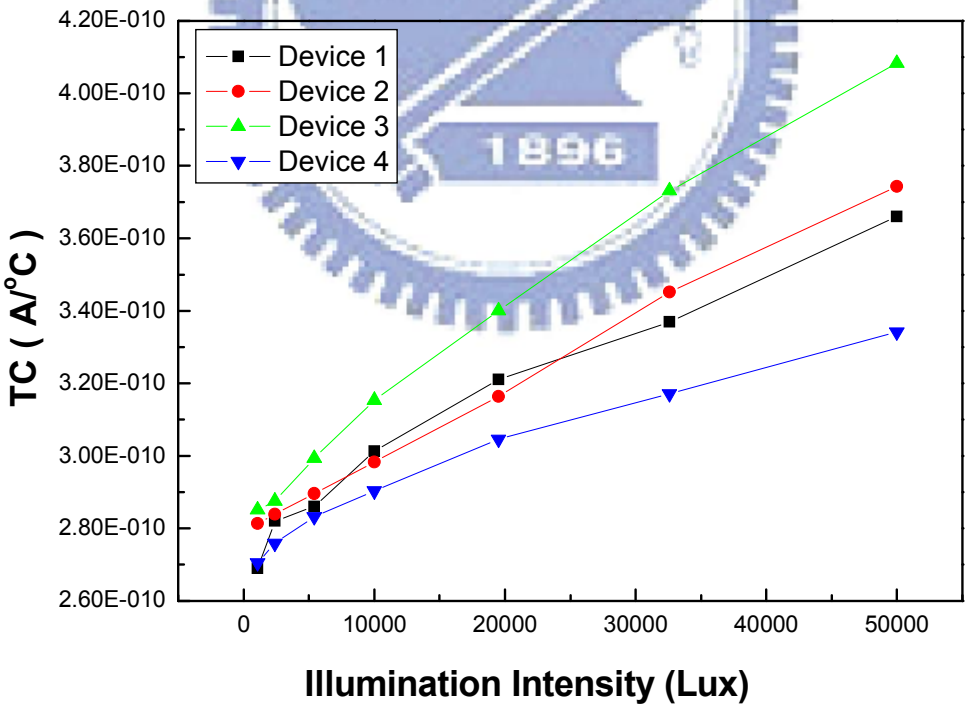

(b)

Fig. 4-4 (a) The drain current versus temperature at Vgs=10V, Vds = 10V and (b) The TC versus temperature curves of 4 devices

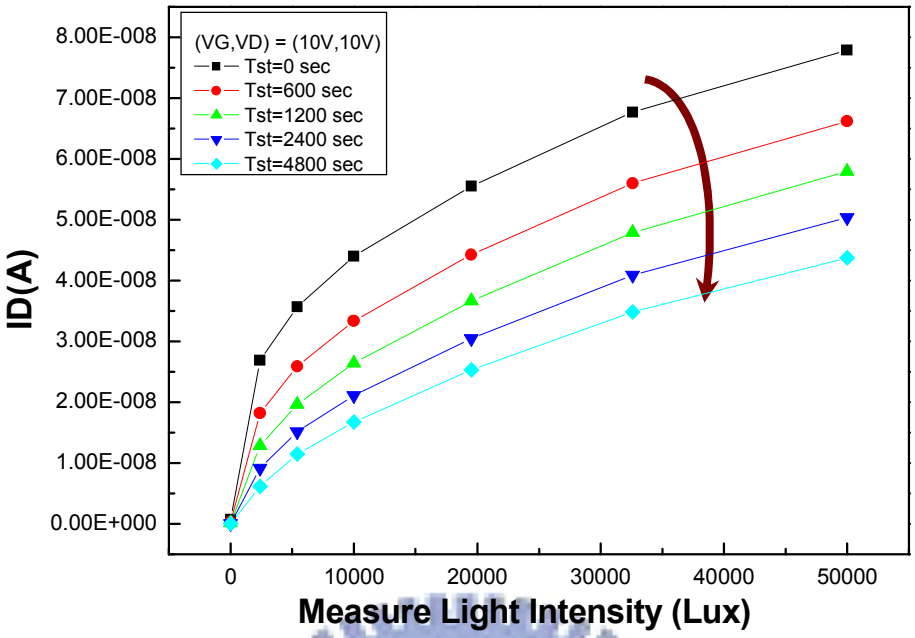

(a)

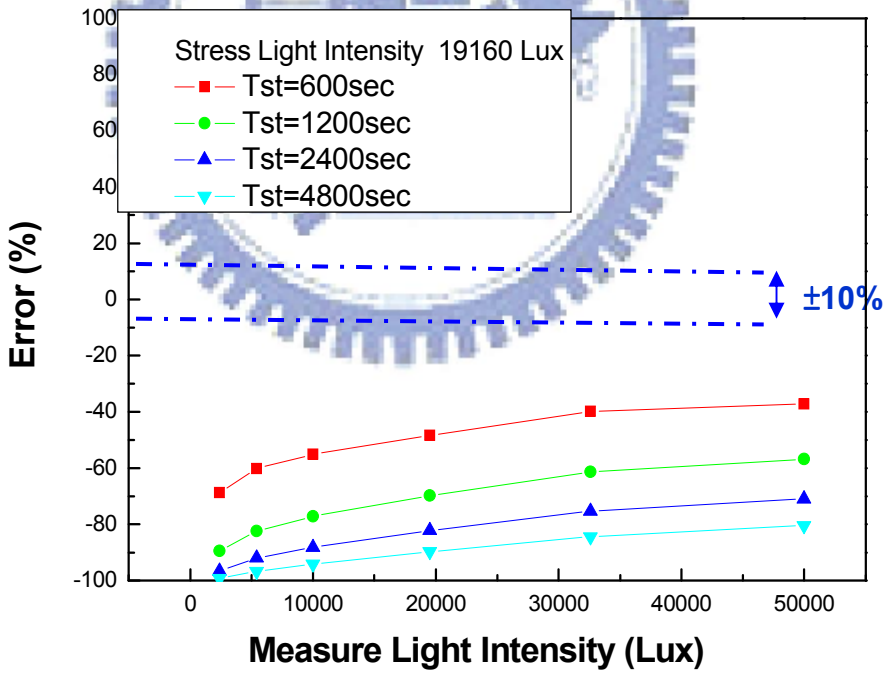

(b)

Fig. 4-5 (a) The drain current versus illumination intensity curves with different optical stress times and (b) Error analysis of SW effect between the measured light intensity and the illuminated intensity

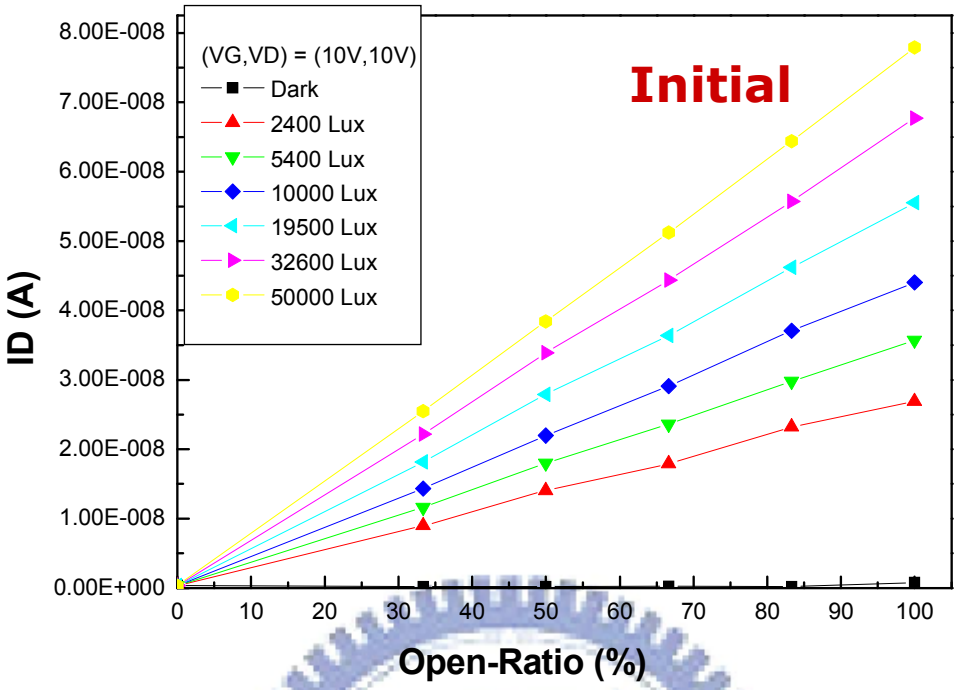

(a)

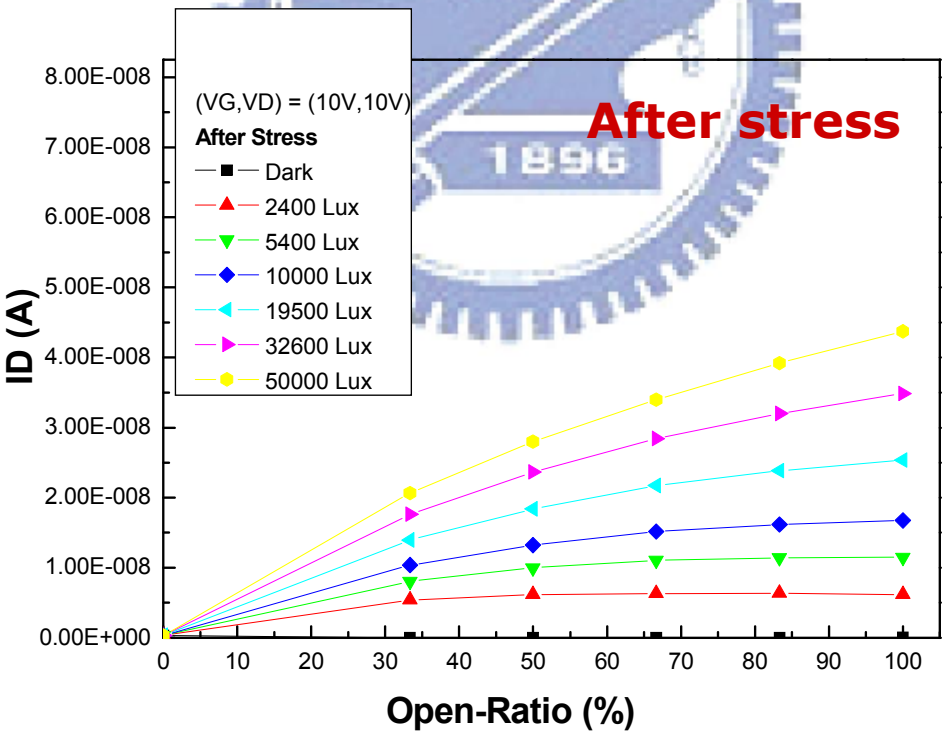

(b)

Fig. 4-6 Drain current versus open ratio (a) before stress (b) after stress

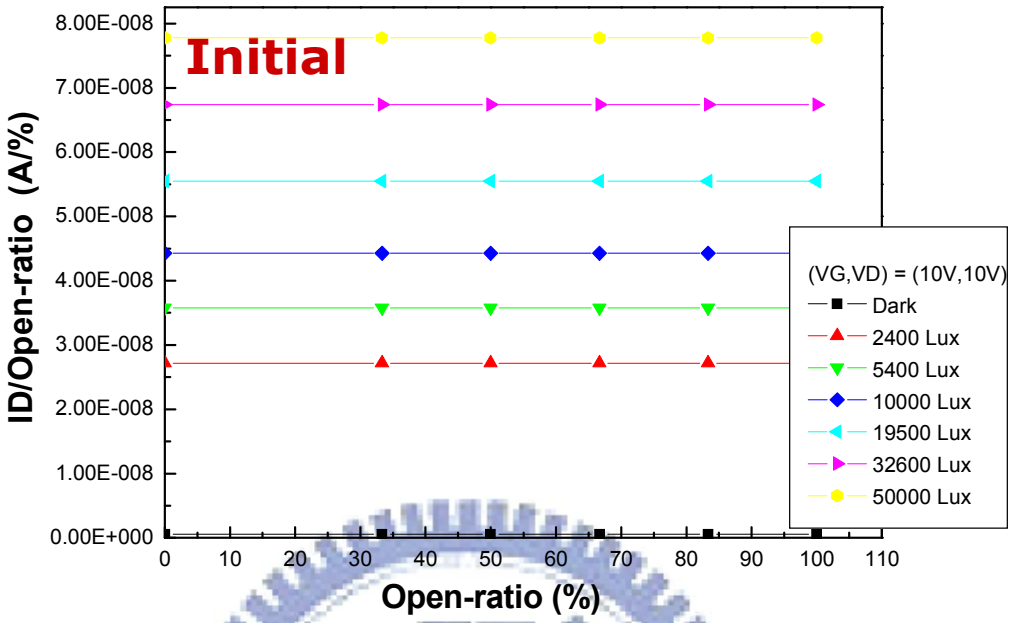

(a)

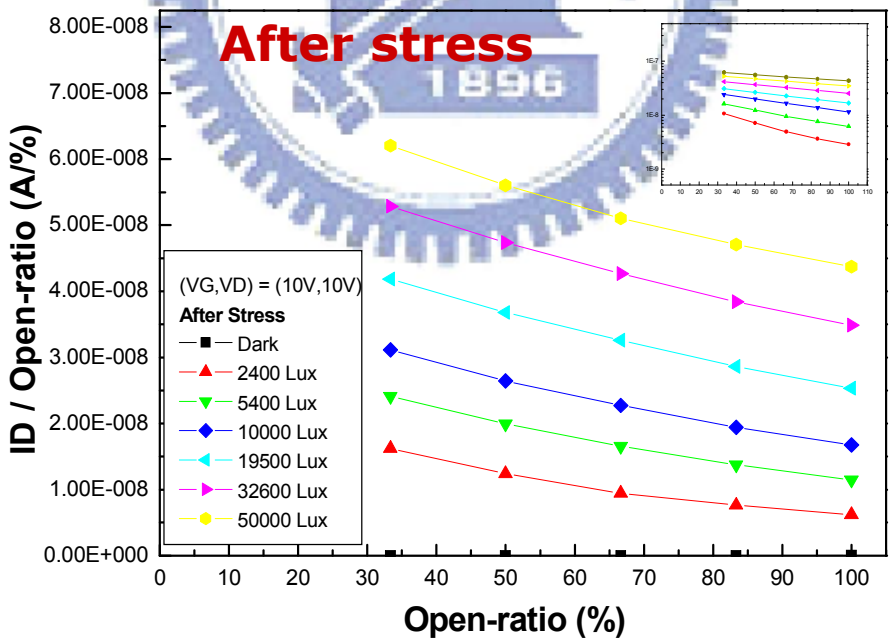

(b)

Fig. 4-7 I_D/Open-ratio versus open-ratio (a) before stress and (b) after stress

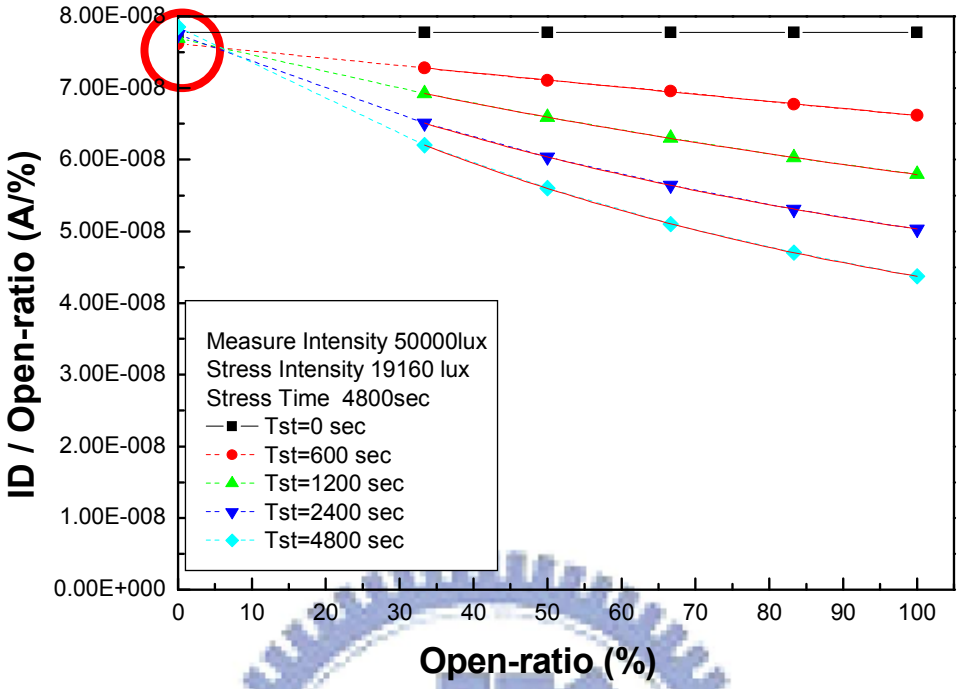

Fig. 4-8 I_D/Open-ratio versus open-ratio under 50000 lux illumination with different stress times

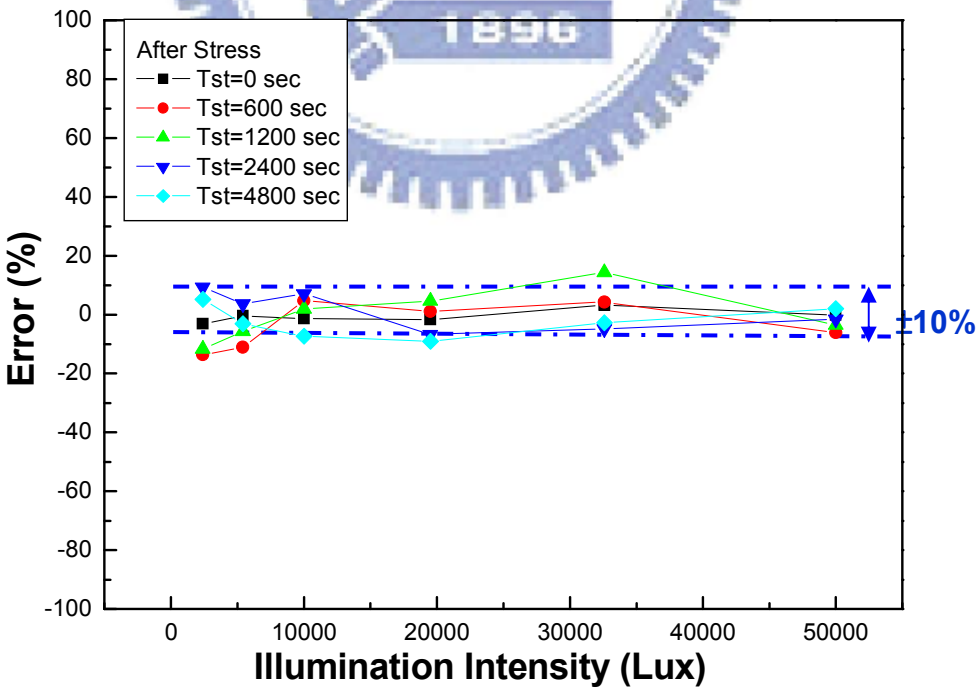

Fig. 4-9 Error analysis of SW effect after calibration between the measured light intensity and the illuminated light intensity

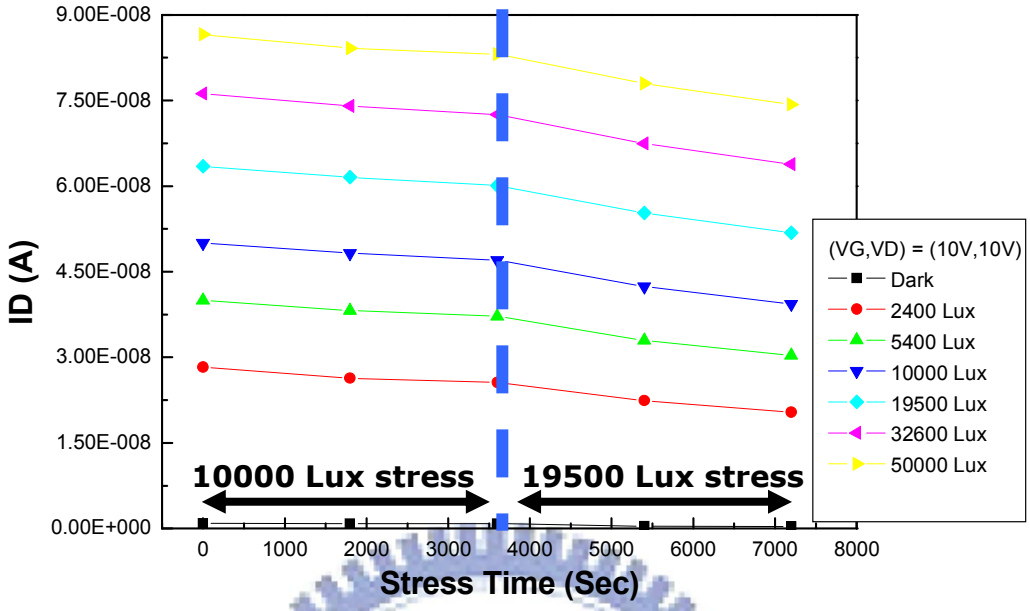

(a)

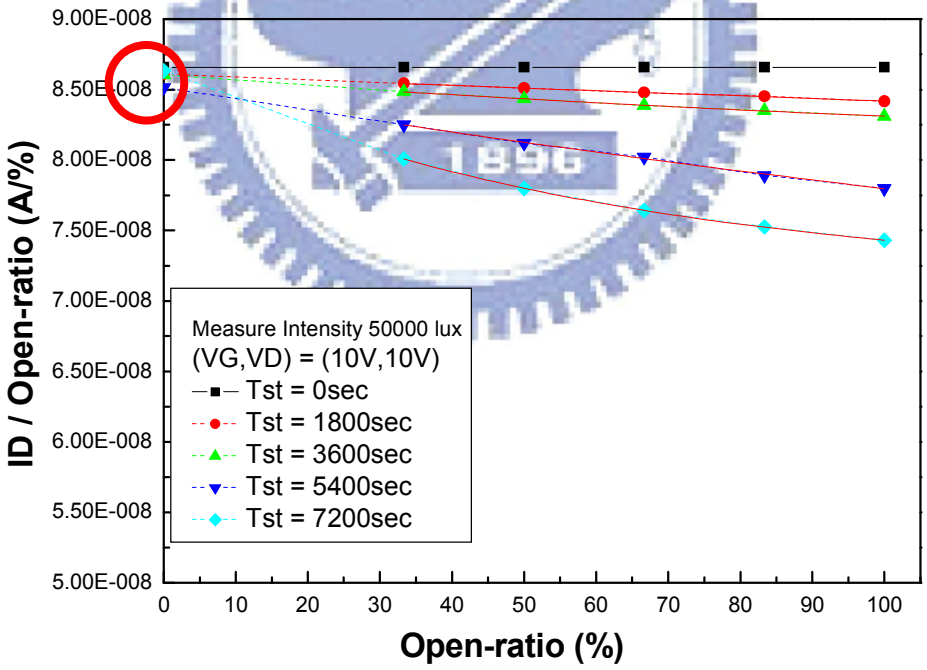

(b)

Fig. 4-10 (a) Optical stress with different light intensities and (b) I_D/Open-ratio versus open-ratio under 50000 lux illumination with different stress times and different stress light intensities

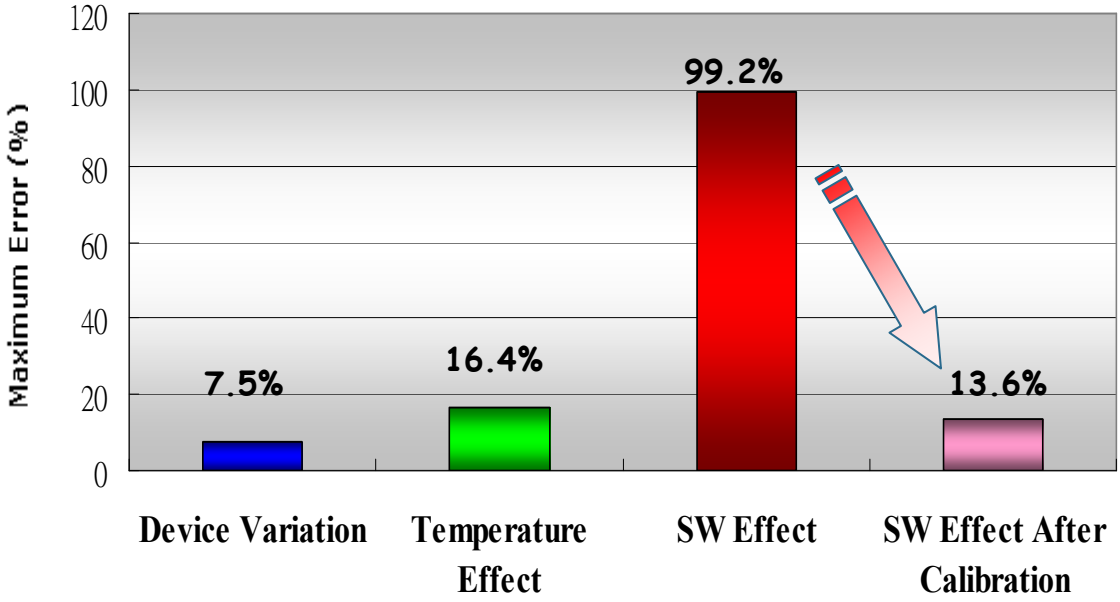

Fig. 4-11 Comparison of the maximum error from each factors

Stress Time	a	b	c	R^2
600sec	7.62E-08	1.98E-07	1922	0.99993
1200sec	7.69E-08	4.04E-08	157	0.99943
2400sec	7.75E-08	4.15E-08	94	0.99986
4800sec	7.85E-08	4.94E-08	82	0.9996

Table 4-1 The fitting parameter of the proposed model at 50000 lux stress intensity.

CHAPTER 5

Conclusion

In this thesis, we use a non-conventional TFT, namely, the gap-type structure, to be the backlight sensing device. We take advantage of its higher current level and good photosensitivity in ON region to sense light intensity. We proposed a light sensing circuit which is designed to be integrated into pixel, and it is compatible to panel's scan lines. The circuit simulation result by H-spice is quite as we expect. Moreover, we analyze the possible factors that can affect the sensing accuracy. We find that SW effect is the most serious problem. Nevertheless, it can be reduced significantly by proposed calibration method.

There are some issues are worthy to be discussed continually. Firstly, we must implant the proposed 4T2C light sensing circuit and verify its feasibility. Then, we need to consider the process of sensor output signals. How to compensate the backlight intensity according to the senor is the main goal of this study. In this thesis, we discussed base on the white LED backlight illumination. We also need to consider the RGB LED backlight since the photosensitivity of a-Si TFT is different under various wavelength light illumination. Therefore, it still has many issues should be researched continually for application.

References

[1] M. Katayama, “TFT-LCD technologe” ELSEVIER, 1999, 140-147

[2] B.-D. Choi and O.-K. Kwon, “Stepwise data driving method and circuits for low-power tft-lcds” IEEE , 2000, pp. 1155-1160

[3] C.C. Lai, C.C. Tsai, “Backlight Power Reduction and Image Contrast Enhancement Using Adaptive Dimming for Global Backlight Application” IEEE, 2008, pp. 669-674

[4] M. Anandan, “LED Backlight: Enhancement of picture quality on LCD screen” ASID, 2006,pp.130-134

[5] M.Zeiler, L. Plötz, W. Schwedler and H. Ott,"Highly Efficient LED Backlight Solutions for Large LCDs," Digest, 2005, 57

[6] W. den Boer et al. “Active Matrix LCD with Integrated Optical Touch Screen” SID, 2003, pp.1494–1497

[7] A. Abileah et al. “Interated Optical Touch Panel in a 14.1” SID, 2004, pp.1544-1577

[8] S.H. Kim, E.B. Kim, H.Y. Choi, M.H. Kang, J.H. Hur, J. Jang, ‘A coplanar hydrogenated amorphous silicon thin-film transistor for controlling backlight brightness of liquid-crystal display’ Solid-State Electronics, 2007, pp.478-481

[9] S. M. GadelRab, S.G. Chamberlain, “The Source-Gated Amorphous Silicon Photo-Transistor” IEEE, 1997, pp.1789-1794

[10] J.D. Gallezot, S. Martin, J. Kanicki, “Photosensitivity of a-Si:H TFTs” AMD, pp.407-411

[11] T. SHIMIZU “Staebelr-Wronski Effect in Hydrogenated Amorphous Silicon And Related Alloy Films” Japan Society of Applied Physics, 2004, pp.3256-3268

[12] W.D. Boer, A. Abileah, P. Green, T. Larsson, “Active Matrix LCD with

Integrated Optical Touch Screen" SID Tech. Dig., 2003, pp. 1494-1497.

[13] B.T. Chen, Y.H. Tai, K.F. Wei, C.C. Tsai, C.Y. Huang, Y.J. Kuo, H.C. Cheng "Investigation of source-follower type analog buffer using low temperature poly-Si TFTs" Solid-State Electronics, 2007, vol. 51, pp. 354-359.

[14] G-Y. Yang, Y-G. Kim, T-S. Kim, J-T. Kong, "S-TFT: An Analytical Model of Polysilicon Thin-Film Transistors for Circuit Simulation" IEEE Custom Integrated Circuits Conference, 2000, pp.213-316.

[15] MARTIN J. POWELL "The Physics of Amorphous Silicon Thin Film Transistors" IEEE, 1989, 2753-2763.

[16] W.S. Lee, G.W. Neudeck, J. Choi, S. Luan, "A Model for the Temperature-Dependent Saturated ID-VD Characteristics of an a-Si:H Thin-Film Transistor" IEEE, 1991, pp.2070-2074.

[17] M. Vanecek, A. Poruba, A. Fejfar, J. Kocka, "Dircet measurement of the deep defect density in thin amorphous silicon films with the absolute constant photocurrent method" Japan Society of Applied Physics, 1995, pp.6203-6210.

[18] T. Kruger, "On the origin of the Staebler-Wronski effect" Japan Society of Applied Physics, 2006.

[19] L. Eglseer, S. Horvat, H. Kroha, 'Study of the long-term behavior of the sensitivity of amorphous silicon photo detectors under illumination' ELSEVIER, 2006.

[20] A. Colin Cameron, Frank A. G. Windmeijer, ' R-Squared Measures for Count Data Regression Models With Applications to Health-Care Utilization' Journal of Business & Economic Statistics, 1996, pp.209-222.